Top Curr Chem (2016) 368: 219–272
DOI: 10.1007/128_2014_616

Published online: 10 April 2015

Dynamical Processes in Open Quantum Systems from a TDDFT Perspective: Resonances and Electron Photoemission

Ask Hjorth Larsen, Umberto De Giovannini, and Angel Rubio

Abstract We present a review of different computational methods to describe time-dependent phenomena in open quantum systems and their extension to a density-functional framework. We focus the discussion on electron emission processes in atoms and molecules addressing excited-state lifetimes and dissipative processes. Initially we analyze the concept of an electronic resonance, a central concept in spectroscopy associated with a metastable state from which an electron eventually escapes (electronic lifetime). Resonances play a fundamental role in many time-dependent molecular phenomena but can be rationalized from a time-independent context in terms of scattering states. We introduce the method of complex scaling, which is used to capture resonant states as localized states in the spirit of usual bound-state methods, and work on its extension to static and time-dependent density-functional theory. In a time-dependent setting, complex scaling can be used to describe excitations in the continuum as well as wave packet dynamics leading to electron emission. This process can also be treated by using open boundary conditions which allow time-dependent simulations of emission processes without artificial reflections at the boundaries (i.e., borders of the simulation box). We compare in detail different schemes to implement open boundaries, namely transparent boundaries using Green functions, and absorbing boundaries in

A.H. Larsen (✉) and U. De Giovannini (✉)
Nano-bio Spectroscopy Group and European Theoretical Spectroscopy Facility (ETSF),
Centro de Física de Materiales CSIC-UPV and DIPC, Universidad del País Vasco UPV/EHU,
E-20018 Donostia–San Sebastián, Spain
e-mail: asklarsen@gmail.com; umberto.degiovannini@gmail.com

A. Rubio (✉)
Nano-bio Spectroscopy Group and European Theoretical Spectroscopy Facility (ETSF),
Centro de Física de Materiales CSIC-UPV and DIPC, Universidad del País Vasco UPV/EHU,
E-20018 Donostia–San Sebastián, Spain

Max Planck Institute for the Structure and Dynamics of Matter, Hamburg, Germany
e-mail: angel.rubio@ehu.es

the form of complex absorbing potentials and mask functions. The last two are regularly used together with time-dependent density-functional theory to describe the electron emission dynamics of atoms and molecules. Finally, we discuss approaches to the calculation of energy and angle-resolved time-dependent pump–probe photoelectron spectroscopy of molecular systems.

Keywords Absorbing boundaries · Complex scaling · Photoemission · Resonances

Contents

1 Introduction

All natural phenomena occur away from equilibrium. Non-equilibrium systems can range in scale from microscopic (such as nanostructures and bacteria) to geological phenomena, and away-from-equilibrium processes occur on timescales ranging from nanoseconds to millennia. Despite the ubiquitous non-equilibrium systems and processes, most of the current understanding of physical and biological systems is based on equilibrium concepts. In fact, in interacting many-body systems, more

often than not we face the fact that the electronic states have finite lifetimes because of the coupling to the environment or to a continuum of states (*resonance processes*). Even if we were able to prepare a perfectly isolated quantum system, we would need to regard a measurement of the system as bringing the system into contact with an environment. Already a single atom in vacuum cannot be regarded as completely isolated, because the atom is embedded in the surrounding photon field (spontaneous emission). Other examples where the coupling to the surrounding plays a prominent role include hot electron relaxation in bulk systems and surfaces after laser irradiation, thermalization caused by electron–phonon coupling, decoherence in pump–probe experiments, exciton propagation and relaxation in biological chromophores, and vibrational relaxation in nanomaterials and molecular systems. Understanding these decay mechanisms provides important information about electron correlations, quantum coherence, dissipative and decoherence processes, and control of these processes has important implications. For instance, this would make it possible to enhance the performance of molecular/solid-based optoelectronic devices.

In this context, density-functional theory (DFT) provides an exact theoretical framework which could yield observable quantities directly, by-passing the need to calculate the many-body wavefunction Ψ. Hohenberg and Kohn [1] proved that all observable properties of a static many-electron system can be extracted exactly from the one-body ground-state density alone (*density–potential mapping*). Later, Runge and Gross extended this theorem to time-dependent systems [2]. Time-dependent density-functional theory (TDDFT) is a rigorous reformulation of the non-relativistic time-dependent quantum mechanics of many-body systems. The central theorem of TDDFT is the Runge–Gross theorem which proves a one-to-one correspondence between the time-dependent external potential $\nu_{\text{ext}}(\mathbf{r}, t)$ and the electronic one-body density $n(\mathbf{r}, t)$ for many-body systems evolving from a fixed initial state Ψ_0. This implies that the time-dependent electronic density determines all properties of the interacting many-electron system: all observable properties of a many-electron system can be extracted from the one-body time-dependent density alone [2]. What has made both DFT and TDDFT so successful is the Kohn–Sham scheme [3]: the density of the interacting many-electron system is obtained as the density of an auxiliary system of non-interacting fermions, living in a one-body potential. Because of the excellent balance between the computational load it requires and the accuracy it provides, TDDFT is now a tool of choice for quite accurate and reliable predictions for excited-state properties in solid state physics, chemistry, and biophysics, in both the linear and nonlinear regimes. However, there exist many situations where the electronic degrees of freedom are not isolated but must be treated as a subsystem embedded in an environment, which influences it in a non-negligible way. Those situations go beyond the realm of the original formulation of TDDFT which is meant to tackle the isolated dynamics of electronic systems. It is therefore clear that there is a need to extend density-functional approaches to the realm of open quantum systems to allow us to treat the processes described above.

Burke and co-workers recently introduced a TDDFT approach based on a Kohn–Sham master equation [4], and in recent work this has been pursued by the group of

Aspuru-Guzik [5–7]. This group also proposed a description of open quantum systems in terms of a unitarily evolving closed Kohn–Sham system [7, 8]. The theory of open quantum systems (OQS) mostly deals with the situation where the environment exchanges energy and momentum with the system but particle number is conserved ([9, Chap. 10]). What happens in the case when the environment exchanges particles with the system is an equivalently important problem which has been less developed. Here we intend to review methods developed to address this kind of problem. We describe the theoretical frameworks and approximations that can be used to describe particle exchange.

Solving the problem of describing a system which exchanges electrons with the environment is only half the challenge. In fact, even in the ideal case where one is able to calculate the correct time-dependent wavefunction, one is faced with the additional problem that some observables may require the knowledge of the complete wavefunction or of eigenstates in the continuum. This includes ionization products such as photoelectron spectra and resonance lifetimes/widths, and is also connected to the measurement process of an open system. These problems are even more severe in the case of DFT and TDDFT, where the density is the only physical object, and where finding the explicit density-functional linking to a physical observable is a daunting task.

This review is structured as follows. We first introduce the general concept of resonance in Sect. 2 and describe how it can be observed in many different physical situations. Then in Sect. 3 we introduce the reader to the basic concepts of the complex scaling theory which is one of the most important tools for studying shape resonances in a static framework. In Sect. 4 we review the successful extension of the complex scaling theory to the realm of DFT, including some recent work adapting the method to the time-dependent realm. In Sect. 5 we review several methods for the incorporation of boundary conditions with the TDDFT equations in order to include the dynamic exchange of electrons with an environment/reservoir. We discuss the strategies for describing specific observables in Sect. 6 where we focus on the case of electron photoemission.

Unless otherwise specified, atomic units are used throughout ($\hbar = m_e = e = 4\pi\varepsilon_0 = 1$).

2 Resonances

Consider a system acted upon by an external oscillating force characterized by some energy and corresponding frequency. If the system responds particularly strongly close to a particular frequency, we call that a *resonance* process. The typical textbook case is that of a classical damped harmonic oscillator acted upon by an external sinusoidal force. For each frequency the system responds by oscillating with some amplitude, and the resonances appear as strong narrow peaks in the amplitude.

This simple model has two important properties that are very general to any type of resonance: First, if the oscillatory force is turned off, the resonant oscillation

decays as governed by the damping force, and the rate of decay is proportional to the *width* of the resonance peak. Second, if we consider the *phase* of the oscillation of the system with respect to that of the external force, we see that it shifts quickly by up to π as the energy passes that of the resonance. The rate with which it shifts is inversely proportional to the decay rate.

We mention here a few commonly studied types of resonance in atomic, molecular, and condensed-matter physics:

- Plasmon resonances where the whole electron charge density in a material resonates with incoming light. Surface plasmon resonances are central to the field of plasmonics.
- Scattering resonances where incident electrons interact with an atom or molecule. Near a resonance energy, the electrons couple strongly and the scattering cross-section shows a peak. The process may be understood as the incoming electron becoming temporarily trapped in a metastable state before escaping.
- Asymmetric Fano resonances [10]. These occur when two coupled excitation pathways interfere with each other.
- Autoionizing resonances, wherein a system such as an atom or molecule is unstable with respect to the ejection of one or more electrons. These are similar to those that would be observed in time-resolved spectroscopies and electron scattering experiments as mentioned above.
- Electron transport processes with molecular junctions, where a bias voltage causes electrons to jump from one metallic lead across a metastable state at a molecule, then escapes through another lead. Such processes have, for example, been studied using DFT plus non-equilibrium Green functions represented with atomic basis sets [11–14].
- Adsorption of an atom onto a surface where the continuum states of the surface couple with the discrete atomic states which then become unstable, broadening into resonances. The Newns–Anderson model [15] describes this process for a one-electron adsorbate.

There are many further classes of resonance which we do not mention here. Below we consider only a small class of resonances, namely scattering or autoionizing ones. In this context, a resonance is a metastable quantum mechanical state that the system possesses, and which can be associated with a wavefunction. Below we describe some mathematical properties of such resonances, with the objective of eventually calculating them from static or time-dependent DFT.

2.1 Definition and Properties of Resonant States

Let us consider a typical scattering experiment where an incoming electron is captured by atom and is temporarily trapped before it escapes again. Whereas scattering processes are clearly time-dependent, resonances can nevertheless be captured from time-independent methods as static properties of the system. A conceptually simple method is to study the phase δ of the wavefunction in the

asymptotic region, taking in one dimension the form $\cos(kx+\delta)$. See for instance the simple demonstration by Gellene [16] which we consider again later. A resonance energy and width can be estimated by locating the energy where the phase shift δ changes most rapidly, and the width can be estimated from the maximum rate of change. This intuitively relates the resonance to a strong coupling of the system with continuum states in a narrow energy interval, as we noted in the beginning.

A more mathematically precise way of identifying a resonance is, following the work of Siegert [17], to search for complex energies corresponding to singularities of the scattering cross section. A pole close to the real energy axis would produce a peak in the scattering cross-section for real energies, consistent with a resonance. As noted by Siegert, the corresponding condition on a wavefunction[1] $\psi(r)$ is that far away from the scattering region:

$$\frac{\mathrm{d}\psi(r)}{\mathrm{d}r} = ik\psi(r), \tag{1}$$

with the energy

$$k^2/2 = \varepsilon - i\Gamma/2, \tag{2}$$

where $\varepsilon > 0$ is the real resonance energy, and $\Gamma > 0$ its width. This yields a discrete set of resonant states characterized by being purely outgoing waves. States obeying the boundary condition (1) are frequently called Siegert or Gamow–Siegert states, and they diverge as $r \to \infty$. See, for example, Hatano et al. [18] for a detailed description of resonant states.

Most computational methods in quantum mechanics work in terms of square integrable states, and thus cannot straightforwardly represent a resonance wavefunction. An elegant solution to this problem is the *complex scaling method*, where one uses complex spatial coordinates to suppress the exponential divergence. One thus solves for functions that obey the usual boundary conditions, $\psi(r) \to 0$ for $r \to \infty$. This also has the convenient advantage that the boundary conditions no longer depend on k. The method relies on the properties of analytic functions to transform the Hamiltonian into a non-Hermitian operator whose point spectrum consists exactly of that of the bound states along the negative real axis plus the complex resonance energies which have positive real part and negative imaginary part. The wavefunctions of bound as well as resonance states are square integrable analytic continuations of the original ones. These properties make the complex scaling method a powerful computational tool as it can make use of many existing methods which do not otherwise apply to unbounded scattering states.

[1] We mention for completeness that Siegert worked in a spherical system where the represented quantity is really r times the wavefunction; this however happens to yield the same equation as in the one-dimensional case.

Although the complex scaling method clearly works with any kind of particles in a finite system, here we explicitly assume that we are dealing with electrons temporarily trapped by simple potentials representing atoms or molecules. The electrons eventually tunnel out to a far-away region which we do not wish to represent explicitly in the calculation. We are thus dealing with the specific case of an open quantum system where we only have particles leaving the system.

3 Calculation of Resonances from Complex Scaling

The complex scaling method was initially developed by Aguilar, Balslev, Combes, and Simon [19–21], and is based on a scaling $\mathbf{r} \to \mathbf{r}e^{i\theta}$ of the position variable in the Schrödinger equation. This is referred to as *uniform* complex scaling. Here we review uniform complex scaling in the simple case of independent particles. Most recent work is based on a later generalization called *exterior* complex scaling [22], which we consider later. The following is a rather informal description of complex scaling, focusing on a few important cases. More information can be found in any of the many existing reviews.[23–27]

3.1 Formalism

Consider the standard independent-particle time-independent Schrödinger equation for a finite system:

$$\hat{H}\psi(\mathbf{r}) = \varepsilon\psi(\mathbf{r}). \tag{3}$$

The Hamiltonian is $\hat{H} = -\frac{1}{2}\nabla^2 + v(\mathbf{r})$, where $\nu(\mathbf{r})$ is some reasonably well-behaved potential which approaches zero as $r \to \infty$. Formally, the potential has to be *dilation* or *dilatation analytic* [19], but the method has been applied successfully to potentials that are not, an example of which is the Stark effect [28–30]. For our informal review we only insist that it be *analytic* in relevant parts of the complex plane.

The spectrum of $\hat{H}$ consists of a negative point spectrum corresponding to the bound states, and the continuum $\varepsilon \geq 0$. The goal of complex scaling is to identify resonances associated with positive energies somewhere within the continuum.

The complex scaling operation is implemented by the operator $\hat{R}_\theta$ defined by

$$\hat{R}_\theta\psi(\mathbf{r}) = e^{iN\theta/2}\psi\left(\mathbf{r}e^{i\theta}\right), \tag{4}$$

where N is the number of spatial coordinates on which the scaling is applied (thrice the number of particles in the 3D many-body case). θ, the *scaling angle*, is a fixed

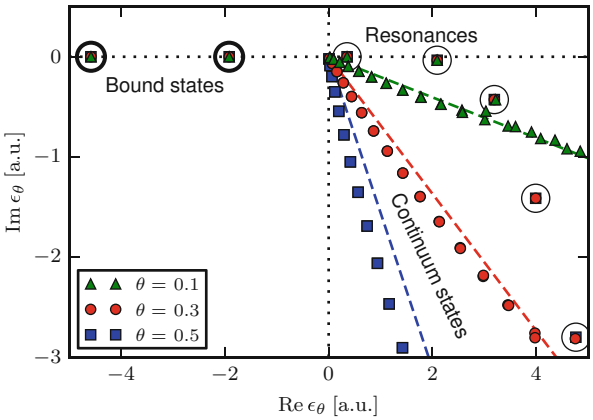

Fig. 1 Effect of complex scaling on the spectrum for the 1D potential $v(x) = 3(x^2 - 2)\exp(-x^2/4)$. Bound-state eigenvalues (*bold circles*) are independent of θ while the continuous spectrum rotates by -2θ around the threshold 0. Because of the finite size of the simulation box, the numerically calculated unbound states (*uncircled*) do not fall exactly on the line $\arg z = -2\theta$. Resonances (*thin circles*) are resolved when θ is sufficiently large for them to segregate from the continuum states. Calculated using a uniform real-space grid from -18 to 18 a.u. with 250 points and fourth-order Laplacian finite-difference stencil

number formally supposed to lie within $0 \leq \theta \leq \pi/4$, although this depends on the analyticity of the potential. The scaling operation transforms the position and momentum operators as $x \to x\mathrm{e}^{i\theta}$ and $\mathrm{d}/\mathrm{d}x \to \mathrm{e}^{-i\theta}\mathrm{d}/\mathrm{d}x$, wherefore the Hamiltonian transforms to

$$\hat{H}_\theta \psi_\theta(\mathbf{r}) = \varepsilon_\theta \psi_\theta(\mathbf{r}) \tag{5}$$

with

$$\hat{H}_\theta = \hat{R}_\theta \hat{H} \hat{R}_\theta^{-1} = -\frac{1}{2}\mathrm{e}^{-i2\theta}\nabla^2 + v\left(\mathbf{r}\mathrm{e}^{i\theta}\right). \tag{6}$$

The transformation maps the potential to its analytic continuation on $\mathbf{r}\mathrm{e}^{i\theta}$ in the complex plane. The interesting property of $\hat{H}_\theta$ is how its spectrum and eigenstates are related to that of $\hat{H}$. First of all, $\hat{H}_\theta$ is non-Hermitian and therefore admits complex eigenvalues. The continuous spectrum "swings down" by an angle of 2θ as shown in Fig. 1. Meanwhile, the energies of any bound states remain unaffected. Finally, for sufficiently large θ, new eigenvalues materialize which are independent of further increase of θ and which are taken to represent resonances. Let us have a closer look at each of these three effects separately.

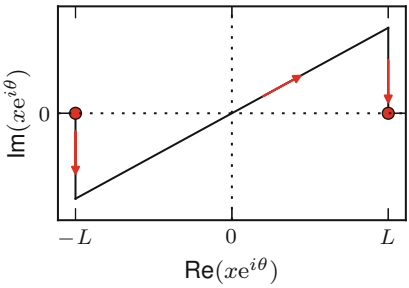

Fig. 2 Complex integration path with directions indicated by *arrows*. If the integrand is suitably localized and analytic on the integration path, the indicated path becomes equivalent to that over the real axis from $-\infty$ to ∞ as $L \to \infty$. This ensures that the unphysical complex scaling angle does not affect matrix elements or expectation values

3.2 Bound States

Suppose $\phi(\mathbf{r})$ and $\psi(\mathbf{r})$ are square-integrable and reasonably well-behaved states. We consider first the scaling operation $\hat{U}_\eta\ \psi(\mathbf{r}) = \mathrm{e}^{N\eta/2}\ \psi(\mathbf{r}\mathrm{e}^{\eta})$ where η is a real number. This operation is easily seen to be unitary; for example it preserves scalar products:

$$\left\langle \phi \middle| \hat{U}_\eta^{\dagger} \hat{U}_\eta \middle| \psi \right\rangle = \int \phi^*(\mathbf{r}\mathrm{e}^{\eta}) \psi(\mathbf{r}\mathrm{e}^{\eta}) \mathrm{d}\mathbf{r}\mathrm{e}^{N\eta} = \int \phi^*(\mathbf{r}') \psi(\mathbf{r}') \mathrm{d}\mathbf{r}' = \left\langle \phi \middle| \psi \right\rangle, \tag{7}$$

where we used the substitution $\mathbf{r}' = \mathbf{r}\mathrm{e}^{\eta}$. A real scaling therefore preserves matrix elements and eigenvalues.

The derivation of the complex scaling method starts with the unitarity of the real scaling, then considers the extension to the complex plane of the scaling parameter η. However, as we see, the situation becomes radically different when the scaling is complex. In order for the method to be correct, the scaling operation must retain some property resembling unitarity to make sure that observables do not arbitrarily change with the scaling parameter. The analytic continuations of functions defined originally on the real axis are not always within the Hilbert space (hence breaking unitarity). However, for suitable states and operators, as we see later, the complex scaling operation corresponds simply to a change of integration path which preserves scalar products. Let us consider a matrix element of some local operator

$$\left\langle \phi \middle| \hat{O} \middle| \psi \right\rangle = \int \phi^*(\mathbf{r}) \hat{O}(\mathbf{r}) \psi(\mathbf{r}) \mathrm{d}\mathbf{r}. \tag{8}$$

This integral is taken for each coordinate axis over all real numbers $-\infty$ to ∞. Imagine now that we liberate each position coordinate and allow it to take complex values. Then, instead, we take the integral over some complex path, such as the one in Fig. 2 with three segments. If the diagonal segment is long enough ($L \to \infty$ in the

figure), and the integrand is analytic and sufficiently localized, then the integral along the vertical segments is zero. Thus the integral over the diagonal $z = x\mathrm{e}^{i\theta}$ is independent of θ and equal to that along the real line:

$$\int \cdot \mathrm{d}x = \lim_{a\to\infty} \int_{-a\mathrm{e}^{i\theta}}^{a\mathrm{e}^{i\theta}} \cdot \mathrm{d}x. \tag{9}$$

The substitution $\mathbf{r}' = \mathbf{r}\mathrm{e}^{i\theta}$ then transforms the integral back so the integration variable is (unlike the integrand) real:

$$\left\langle \phi \middle| \hat{O} \middle| \psi \right\rangle = \int \overline{\phi}_\theta(\mathbf{r}) \hat{O}_\theta(\mathbf{r}) \psi_\theta(\mathbf{r}) \mathrm{d}\mathbf{r}, \tag{10}$$

with

$$\psi_\theta(\mathbf{r}) = \mathrm{e}^{iN\theta/2} \psi\left(\mathbf{r}\mathrm{e}^{i\theta}\right) = \hat{R}_\theta \psi(\mathbf{r}), \tag{11}$$

$$\overline{\phi}_\theta(\mathbf{r}) = \mathrm{e}^{iN\theta/2} \phi^*\left(\mathbf{r}\mathrm{e}^{i\theta}\right) = \left[\hat{R}_{-\theta} \phi(\mathbf{r})\right]^*, \tag{12}$$

$$\hat{O}_\theta(\mathbf{r}) = \hat{O}\left(\mathbf{r}\mathrm{e}^{i\theta}\right) = \hat{R}_\theta \hat{O} \hat{R}_\theta^{-1}. \tag{13}$$

Note how (1) the complex prefactors of $\mathrm{e}^{iN\theta/2}$ from (4) serve to "absorb" exactly the volume element $\mathrm{e}^{iN\theta}$ produced by the variable substitution, and (2) the left states or bras are effectively rotated by $-\theta$. Furthermore, if the unscaled state $\phi(\mathbf{r})$ is real, the cumbersome notation for $\overline{\phi}_\theta(\mathbf{r})$ of (12) can be avoided:

$$\overline{\phi}_\theta(\mathbf{r}) = \phi_\theta(\mathbf{r}) \quad \text{if } \phi(\mathbf{r}) \text{ is real.} \tag{14}$$

We can then calculate the matrix element without conjugating anything.

What we have established is that the complex scaling operation corresponds to a change of integration path when calculating matrix elements. For states and operators that produce a sufficiently localized integrand and do not possess poles that interfere with the integration path, it preserves values of matrix elements. In particular this guarantees that observables or eigenvalues of bound states under complex scaling, at least for sufficiently small values of θ, are independent of θ.

3.3 Continuum States

The previous discussion does not apply to states that are not localized, such as continuum states. Let us consider the complex-scaled Schrödinger equation for a free particle in one dimension:

$$-\frac{1}{2}\frac{\mathrm{d}^2\psi_\theta(x)}{\mathrm{d}x^2}\mathrm{e}^{-i2\theta} = \varepsilon_\theta\psi_\theta(x). \tag{15}$$

We immediately see that this is the *same* differential equation as the unscaled one, and thus has the usual set of solutions:

$$\psi_\theta(x) = A\exp(ikx) + B\exp(-ikx). \tag{16}$$

As per the standard procedure, let us say that the particle is confined to some finite box. We then require that $\psi_\theta(x)$ be 0 on the boundaries, which quantizes k to a set of real positive numbers. Taking the limit of large boxes, we see that solutions exist for all $k > 0$. It follows that the energy ε_θ in (15) must become complex according to

$$\varepsilon_\theta = \frac{1}{2}k^2\mathrm{e}^{-i2\theta}, \quad k > 0. \tag{17}$$

Evidently the spectrum has been rotated by an angle of -2θ into the fourth quadrant of the complex plane. Meanwhile, the solution wavefunctions for the free particle have the same form as without the complex scaling operation.

What, then, is so interesting about the complex-scaled solutions $\psi_\theta(x)$? Because they are not normalizable, and because their energy depends on the scaling angle θ, they are not of much use computationally. However, we can gain some insight by scaling them back to $\theta = 0$ to obtain

$$\hat{R}_{-\theta}\psi_\theta(x) = \mathrm{e}^{-i\theta/2}\left(A\mathrm{e}^{ikx\cos\theta}\mathrm{e}^{kx\sin\theta} + B\mathrm{e}^{-ikx\cos\theta}\mathrm{e}^{-kx\sin\theta}\right). \tag{18}$$

For $x \to \infty$ the right-going term diverges whereas the left-going one dies out. For $x \to -\infty$ it is the left-going one which survives. The solution $\psi_\theta(x)$ to the complex-scaled problem therefore resembles an outgoing, exponentially diverging state. We see intuitively that the complex scaling operation may have something to say about the outgoing character of states. However, as mentioned, the states $\psi_\theta(x)$ are not normalizable and their energies depend on θ. The main effect of the complex scaling operation was to move the continuous spectrum of the Hamiltonian away from the real axis, close to which we find the resonance eigenvalues as we see later.

If the system consists of a central, (almost) localized potential surrounded by vacuum, an unbound state still has the form (16) almost everywhere in space. Importantly and non-trivially, this also works with the Coulomb potential in spite of its long range. The complex scaling transformation still causes the continuous spectrum to rotate by exactly -2θ. In numerical representations this is only approximately true because of incompleteness of the basis and in particular finite simulation boxes as in Fig. 1.

We note here that the method cannot in general be combined with extended (periodic) systems, because complex scaling fundamentally works in terms of the asymptotic form of decaying functions. For example, a metal would possess occupied continuum states which do not decay at the end of the cell. This makes

their properties depend on the scaling angle θ as we saw for free particles. However, from what we have seen so far, one could well imagine using complex scaling in some directions and not others – for example, to describe electrons escaping in the z direction from a surface which is periodic along x and y, or radially from a one-dimensional nanowire.

3.4 Resonant States

From standard scattering theory we know that resonances are associated with wavefunctions that diverge exponentially at increasing distances. If the resonance is generated by a short-range potential, the resonance wavefunction must far away equal or approach that of a free particle.

In one dimension the resonance wavefunction must therefore have the form

$$\psi(x) = A\mathrm{e}^{ikx} = A\mathrm{e}^{i(p-iq)x}, \quad x \to \infty, \tag{19}$$

where we have used the complex wavenumber $k = p - iq$ with positive p (so the wave is outgoing) and q (so it diverges exponentially). Now apply the complex scaling transformation to this function:

$$\hat{R}_\theta \psi(x) = \mathrm{e}^{i\theta/2}\mathrm{e}^{i(p-iq)x\mathrm{e}^{i\theta}} = \mathrm{e}^{i\theta/2}\mathrm{e}^{i(p\cos\theta+q\sin\theta)x}\mathrm{e}^{(-p\sin\theta+q\cos\theta)x}. \tag{20}$$

This function is square integrable if $q < p \tan\theta$. Physically we would expect a resonance peak to be located at a positive energy, and that the resonance width is much smaller than the resonance energy. The energy of this wave is $(p-iq)^2/2 = (p^2 - q^2 - 2ipq)/2$, and we would thus expect p to be well greater than q for any resonance. Some intermediate value of θ therefore easily ensures that $q < p \tan\theta$, i.e., that the resonance wavefunction is square integrable.

We conclude from this that the Siegert wavefunction representing a resonant state indeed becomes square integrable under adequate complex scaling. This makes matrix elements with resonant states invariant to variations in θ, similarly to bound states, as long as the variation of θ does not make them unbounded.[2]

The numerical convergence of resonance energies and widths is a non-trivial issue with complex scaling. When using a numerical representation such as a finite basis set, matrix elements are not perfectly independent of θ. For a given system it is standard practice to compare calculated resonance energies and widths over a range of different θ-values, looking for a stationary point or a cusp which, following the

[2] The above discussion is, of course, very informal. Scrinzi and Piraux have presented a more complete argument on the link between outgoing wavefunctions and square integrability after complex scaling; see Scrinzi and Piraux [31], Appendix A.

"complex virial theorem," would best approximate the fully converged complex energy [32, 33].

3.5 *Exterior Complex Scaling*

We established previously that the complex scaling operation preserves scalar products of square integrable states because it corresponds to a change of integration contour of an analytic function. Suppose we want to calculate a resonance of a molecule in the Born–Oppenheimer approximation. The nuclear point charges cause poles in the Coulomb potential at each nuclear position. Uniform complex scaling does not work because of these poles. A solution to this problem is to change the integration contour to avoid the poles. From complex analysis we know that we could have chosen many other integration paths, corresponding to other definitions of the scaling operation $\hat{R}_\theta$, and those contours would equally well preserve scalar products as long as the integration contours have the same start and end points and do not enclose poles. This is the basis for *exterior complex scaling* which was proposed by Simon [22] to solve exactly this problem. Another method is to use the analytic continuation of matrix elements within a basis set representation [34–36], which effectively approximates the exterior complex scaling approach [37].

We thus complex-scale the *exterior* of a region containing all the point charges by an operation, here written in one dimension, of the form

$$\hat{R}_\theta^a \psi(x) = \begin{cases} \psi\left(-a + (x+a)\mathrm{e}^{i\theta}\right), & x < -a, \\ \psi(x), & -a \le x < a, \\ \psi\left(a + (x-a)\mathrm{e}^{i\theta}\right), & a \le x. \end{cases} \tag{21}$$

The uniform and exterior scaling integration contours are shown in Fig. 3. The important condition for exterior scaling is that the scaling retains the asymptotic form $x \to x\mathrm{e}^{i\theta}$ which ensures outgoing-wave boundary conditions. Because the integration contour is not differentiable, neither is an exterior complex-scaled function that corresponds to a smooth original function. Recall from uniform scaling that we needed to multiply by $\mathrm{e}^{i\theta/2}$ to "absorb" the now complex volume element when integrating. We have not done anything to the volume element in (21), and therefore we need to apply a factor of $\mathrm{e}^{i\theta}$ when calculating integrals over the complex segments. Alternatively, most authors define the exterior scaling operation so the wavefunction in the exterior segments includes the complex prefactor; the functions then become discontinuous [38], but we do not need to consider the volume element when integrating. Here we have followed the original convention of Simon [22] where the function is always continuous. As long as the discontinuities of the complex-scaled functions or their derivatives are well incorporated into the numerical basis set used to represent them, they are harmless.

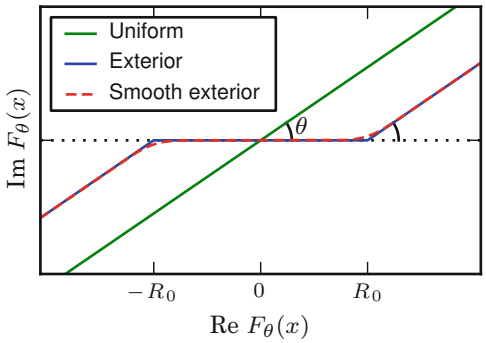

Fig. 3 Possible complex integration contours for uniform, exterior and smooth exterior complex scaling. $\theta = 0.6$. The contours must be continuously deformable (without crossing any poles) back to the real axis in order for them to be equivalent to a real integration. Note that, as per basic complex analysis, the contours themselves do not have to be differentiable – it is sufficient that the integrand be analytic

If for numerical reasons we want smooth functions everywhere, we can equally well choose a smooth integration contour. This is called *smooth-exterior* complex scaling. The scaling operator here acts by applying a smooth function $x \to z = F(x)$ to the position coordinate, with $F(x) \sim x e^{i\theta}$ for large $|x|$.

Once again we have the choice of where to include the smoothly varying volume element: either in the definition of the scaling operation, or explicitly when integrating. This yields different expressions which are given, for example, by Moiseyev [39]. If we include the volume element in the scaling operation, it reads

$$\hat{R}^{F}_{\text{smooth}}\psi(x) = [F'(x)]^{1/2}\psi(F(x)). \tag{22}$$

The Hamiltonian subject to this transformation is

$$H^F = -\frac{1}{2}[F'(x)]^{-2}\frac{\partial^2}{\partial x^2} + V_1^F(x)\frac{\partial}{\partial x} + V_0^F(x) + V[F(x)], \tag{23}$$

where

$$V_0^F(x) = \frac{1}{4}[F'(x)]^{-3}F'''(x) - \frac{5}{8}[F'(x)]^{-4}[F''(x)]^2, \tag{24}$$

$$V_1^F(x) = [F'(x)]^{-3}F''(x). \tag{25}$$

An example contour is shown in Fig. 3. The contour defined by F can be quite general, but one would choose $F(x) = x$ within the interior region such that $V_0^F(x) = V_1^F(x) = 0$ and $[F'(x)]^{-2} = 1$. Note how (23) then reduces to the usual Schrödinger equation as it should. With this formulation we do not need to mind

any discontinuities of wavefunctions, their derivatives, or the Jacobian, and standard methods such as finite-difference stencils can be applied straightforwardly as long as F is adequately differentiable.

How do the different types of complex scaling discussed above compare computationally? The basic equations of exterior and smooth exterior complex scaling are clearly more complicated than those for uniform scaling. However, as mentioned, the purpose of exterior complex scaling is that it admits potentials that are not analytic within the interior region. This includes any strictly localized function such as most atomic pseudopotentials – a major advantage for advanced self-consistent field methods such as DFT. One other advantage of exterior scaling is that. within the interior region, quantities such as the density retain their true physical values rather than a difficult-to-interpret complex continuation which is also numerically difficult to rotate back to real space.

For real-space methods, an advantage of smooth exterior complex scaling is that one can transparently use finite-difference stencils as per (23). Standard finite-difference stencils, representing, for instance, the kinetic operator, do not work on a non-differentiable contour although one can derive special stencils for this case [40]. Basis sets should also make sure to take the discontinuity into account. Finite-element representations involving some kind of basis are commonly used; see, for example, Rescigno et al. [41] and Scrinzi and Elander [42]. Rescigno and co-workers have reported that finite-element calculations with a basis set which properly takes the discontinuity of "sharp" exterior scaling into account require less functions than a purely analytic basis set using smooth scaling [41]. A more detailed discussion of the numerical representations and basis sets can be found in work by McCurdy et al. [24], who also argue that grid-based methods enjoy a similar advantage with sharp exterior complex scaling, provided the scaling onset is exactly on a grid point.[3]

3.6 Example: Resonance in One Dimension

Let us perform an analytic calculation of a resonance using complex scaling to see how exactly the resonance emerges. We consider a barrier formed by the piece-wise constant potential

[3] This would be less of an advantage in Cartesian 3D calculations where a smooth scaling could be applied spherically, whereas the sharp scaling would need a cube to align its boundary with the grid.

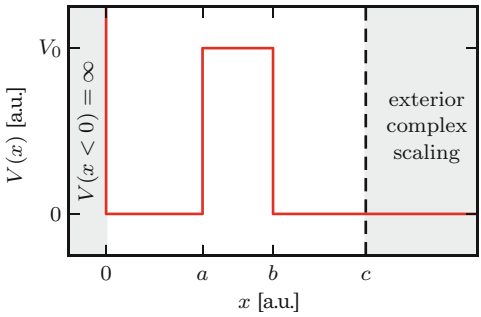

Fig. 4 Rectangular potential barrier supporting resonances. Exterior complex scaling ensures that resonance wavefunctions localize and appear as eigenstates of the scaled Hamiltonian

$$V(x) = \begin{cases} 0, & 0 \leq x < a, \\ V_0, & a \leq x < b, \\ 0, & b \leq x, \end{cases} \tag{26}$$

seen in Fig. 4. Both Gellene [16] and Simons [43] have considered this problem previously. As the rectangular barrier is not an analytic function, we cannot use uniform complex scaling. However, nothing stops us from using exterior scaling, with the scaling transformation starting somewhere outside the barrier at $x = c > b$.

We thus use the contour

$$F_\theta^c(x) = \begin{cases} x, & 0 \leq x < c, \\ c + \mathrm{e}^{i\theta}(x - c), & c \leq x. \end{cases} \tag{27}$$

For $x \geq c$ the Hamiltonian is therefore $-\frac{1}{2}\mathrm{e}^{-i2\theta}\frac{\mathrm{d}^2}{\mathrm{d}x^2}$. This gives us four regions, within each of which the wavefunction must be a solution to the Schrödinger equation for a free particle but with different local momenta k_1, k_2, and k_3^θ which may be complex:

$$\psi_1(x) = -iA\left(\mathrm{e}^{ik_1 x} - \mathrm{e}^{-ik_1 x}\right) = 2A \sin(k_1 x), \quad 0 \leq x < a, \tag{28}$$

$$\psi_2(x) = C\mathrm{e}^{ik_2 x} + D\mathrm{e}^{-ik_2 x}, \quad a \leq x < b, \tag{29}$$

$$\psi_3(x) = F\mathrm{e}^{ik_1 x} + G\mathrm{e}^{-ik_1 x}, \quad b \leq x < c, \tag{30}$$

$$\psi_4^\theta(x) = I\mathrm{e}^{ik_3^\theta x} + J\mathrm{e}^{-ik_3^\theta x}, \quad c \leq x. \tag{31}$$

The expression for $\psi_1(x)$ has been chosen to fulfill the boundary condition $\psi_1(0) = 0$, and A eventually determines the normalization of the state. To relate the three wavenumbers k_1, k_2, and k_3^θ, we note that applying the Hamiltonian to the wavefunction must yield the same energy eigenvalue $\varepsilon_\theta = k_1^2/2 = k_2^2/2 + V_0 = \left(\mathrm{e}^{-i\theta}k_3^\theta\right)^2/2$ within each segment. From this may take $k_3^\theta = k_1\mathrm{e}^{i\theta}$.

The segments must be joined continuously and differentiably, i.e., $\psi_1(a) = \psi_2(a)$ and $\psi_1'(a) = \psi_2'(a)$ at $x = a$. Likewise $\psi_2(b) = \psi_3(b)$ and $\psi_2'(b) = \psi_3'(b)$. At $x = c$,

the onset of the scaled exterior region, the derivative $\psi'_3(c)$ must match the *scaled* derivative $\psi_4^{\theta\,\prime}(c)$, so the derivative becomes discontinuous [22]:

$$\psi_3(c) = \psi_4^{\theta}(c), \tag{32}$$

$$\psi'_3(c) = \mathrm{e}^{-i\theta}\psi_4^{\theta\prime}(c). \tag{33}$$

(We have here, for esthetic reasons, chosen not to include the square root of the volume element or Jacobian in the definition of $\psi_4^{\theta}(x)$; if we had, the function itself would have been discontinuous as discussed in Sect. 3.5.)

We thus have two equations at each of the points a, b, and c, for a total of six equations. A seventh equation follows from the requirement that the function be square integrable. These seven equations determine the six unknown coefficients C, D, F, G, I, and J, and further quantize the energy so that we get solutions only for specific wavenumbers k_1, k_2, and k_3^{θ}.

Gellene [16] provides expressions for the coefficients C, D, F, and G in terms of A so that $\psi_1(x)$, $\psi_2(x)$, and $\psi_3(x)$ match at the points a and b. The resonances are then found by considering the phase shift between the incoming and outgoing coefficients F and G of $\psi_3(x)$. However, this is very different in our case using complex scaling; here, the coefficients I and J of $\psi_4^{\theta}(x)$ must ensure square integrability.

Physically, we would expect of a resonance that its energy is much greater than its width. The wavenumber k_1 then has real and imaginary parts $k_1 = p - iq$ such that $p \gg q$. The wavefunction can thus be written as

$$\begin{aligned}\psi_4^{\theta}(x) = {} & I\mathrm{e}^{(-p\sin\theta+q\cos\theta)x}\mathrm{e}^{i(p\cos\theta+q\sin\theta)x} \\ & +J\mathrm{e}^{(p\sin\theta-q\cos\theta)x}\mathrm{e}^{-i(p\cos\theta+q\sin\theta)x}.\end{aligned} \tag{34}$$

For scaling angles θ not too close to zero, the first term converges whereas the second diverges as $x \to \infty$, and so we conclude that $J = 0$. Relating the right and left values and derivatives of $\psi_3(x)$ and $\psi_4^{\theta}(x)$ at $x = c$ we get

$$F\mathrm{e}^{ik_1c} + G\mathrm{e}^{-ik_1c} = I\mathrm{e}^{ik_1\mathrm{e}^{i\theta}c}, \quad \text{(values)} \tag{35}$$

$$ik_1\left(F\mathrm{e}^{ik_1c} - G\mathrm{e}^{-ik_1c}\right) = ik_1I\mathrm{e}^{ik_1\mathrm{e}^{i\theta}c}, \quad \text{(derivatives)} \tag{36}$$

and it immediately follows that $G = 0$, i.e., there is no incoming wave component. This is very different from the Hermitian treatment demonstrated by Gellene which yields $F = G^*$, exactly balancing the outgoing and incoming flux. We see that, as previously discussed, the square integrability requirement of the complex-scaled solution ensures that waves are purely outgoing. In a simple model we could just as easily have forgotten everything about complex scaling and set $G = 0$ immediately. However, in a numerical calculation things are not so simple, and we have to rely on the complex scaling transformation to ensure square integrability and to extract the resonant states in a tractable form.

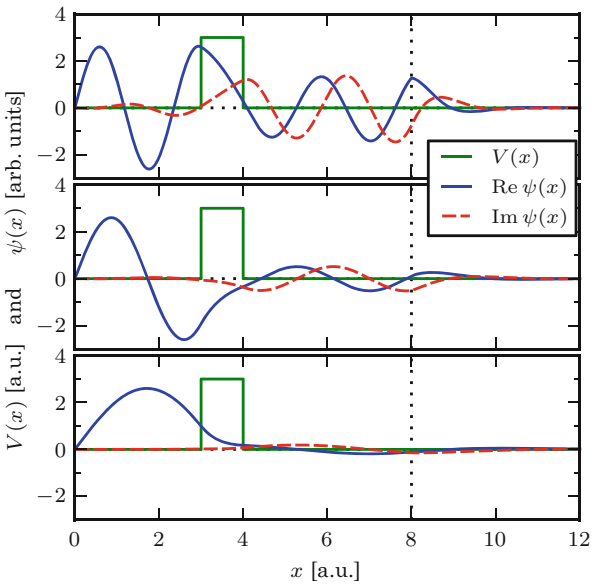

Fig. 5 The first (*bottom*), second (*middle*), and third (*top*) lowest-energy resonances of the model potential. Exterior scaling is applied for $x \geq 8$ which exponentially damps the resonance wavefunctions. Otherwise they would be exponentially increasing

In a more complicated potential generated by multiple atoms, the situation would be similar sufficiently far away from the system. The asymptotic form of the wavefunctions may differ slightly because of long-range interactions such as the Coulomb interaction, but this doesn't prevent the exponentially localizing effect of the complex scaling operation from functioning.

However, let us get back to the determination of the resonance eigenvalues. The requirement that $G = 0$ allows us to proceed, linking F, D, and C by means of the differentiability and continuity requirements. Once all coefficients are eliminated, the condition for resonance is

$$\left(1 - \frac{k_2}{k_1}\right)\left(\tan k_1 a - i\frac{k_1}{k_2}\right)\mathrm{e}^{2ik_2(b-a)} + \left(1 + \frac{k_2}{k_1}\right)\left(\tan k_1 a + i\frac{k_1}{k_2}\right) = 0. \qquad (37)$$

For any energy $\varepsilon - i\Gamma/2$, the wavenumbers k_1 and k_2 are uniquely determined. The solutions can then be determined numerically. The three complex resonance energies closest to 0 are given by the real parts $\varepsilon = 0.421$, 1.65, 3.57, and half-widths $\Gamma/2 = 0.00138$, 0.0189, 0.138. Figure 5 shows the corresponding resonance wavefunctions. The eigenvalues slightly disagree with those by Gellene who works effectively on the real axis. This is because the two methods are different: With complex scaling we find an eigenvalue in the complex plane which corresponds exactly to an outgoing wave. Working on the real axis, we would find the real energy which responds most strongly to that eigenvalue. However, as the complex eigenvalue gets further away from the real axis, location and width soon begin to differ.

4 Density Functional Resonance Theory

As the complex scaling formalism is based on the many-particle Schrödinger equation, the method inherits the same exponential computational cost with respect to the number of particles. The method in the original form is therefore practical only for systems with very few particles, such as small atoms or molecules, using, for example, correlated basis sets [44, 45]. However, larger systems require more scalable computational methods, of which many have been investigated. Of particular interest are self-consistent field methods such as Hartree–Fock [46], post-Hartree–Fock methods [47, 48], and DFT [49, 50]. DFT as always has the drawback that it relies on a complicated formalism including an approximation of the exchange and correlation effects which is difficult to control, but its inarguable performance advantages nevertheless make it more than worthy of consideration. Below we describe the extension of DFT with complex scaling.

4.1 Complex Scaling and DFT

DFT is based on the minimization of a functional of the real electron density. The minimum of the functional and the corresponding electron density are the ground-state energy and electron density [1, 3]. For practical calculations one uses a set of single-particle states or Kohn–Sham states to facilitate evaluation of the kinetic part of the functional. The Kohn–Sham energy functional contains the following contributions: the kinetic energy, the Hartree energy, the exchange–correlation (XC) energy, and the energy from a system-dependent external potential. The kinetic energy functional depends explicitly on the Kohn–Sham wavefunctions whereas the others depend on them only through the density. Either way, all the terms can be understood as sums of matrix elements of operators. We know from Sect. 3.2 how the complex scaling operation conserves matrix elements of states that are spatially localized, provided that the operators are analytic. We can therefore reasonably expect complex scaling to be made to work within DFT, once we know how each term in the energy functional scales. The combination has been dubbed density functional resonance theory (DFRT) [50].

One would thus propose a complex-valued energy functional

$$E_\theta = -\frac{1}{2}\mathrm{e}^{-i2\theta}\sum_n f_n \int \overline{\psi}_{\theta n}(\mathbf{r})\nabla^2\psi_{\theta n}(\mathbf{r})\mathrm{d}\mathbf{r} + \frac{1}{2}\mathrm{e}^{-i\theta}\int\int \frac{\rho_\theta(\mathbf{r})\rho_\theta(\mathbf{r}')}{\|\mathbf{r}-\mathbf{r}'\|}\mathrm{d}\mathbf{r}\mathrm{d}\mathbf{r}' + E_{\mathrm{xc}}^{\theta}[n_\theta] + \int v_{\mathrm{ext}}\left(\mathbf{r}\mathrm{e}^{i\theta}\right)n_\theta(\mathbf{r})\mathrm{d}\mathbf{r} \tag{38}$$

with the complex-scaled density

$$n_\theta(\mathbf{r}) = \sum_n f_n \overline{\psi}_{\theta n}(\mathbf{r}) \psi_{\theta n}(\mathbf{r}) \mathrm{d}\mathbf{r} = \mathrm{e}^{iN\theta} n\left(\mathbf{r}\mathrm{e}^{i\theta}\right), \tag{39}$$

where f_n are occupation numbers, and N the number of dimensions in which the coordinates are complex-scaled. In (38) the kinetic and external contributions are complex-scaled as normal. In the Hartree energy, $\rho_\theta(\mathbf{r})$ denotes the complex-scaled charge density which is the electron density $n_\theta(\mathbf{r})$ plus any other contributions such as pseudopotential charges (whose complex-scaled form is uniquely determined by requiring that their Hartree potential scales as normal). The Hartree energy itself scales as $E_{\mathrm{H}}^\theta[n_\theta] = \mathrm{e}^{-i\theta} E_{\mathrm{H}}[n_\theta]$, i.e., the standard Hartree functional is applied to the *complex* density, with the factor $\mathrm{e}^{-i\theta}$ appearing because of the $1/r$ kernel. We discuss the complex XC energy functional $E_{\mathrm{xc}}^\theta[n_\theta]$ later.

Being complex, "minimizing" the energy functional (38) does not strictly make sense. Nevertheless, the lowest-energy resonance is obtainable as a stationary point of the complex energy functional [51]. An equation for the stationary point can, as normal, be obtained by taking the derivative with respect to the wavefunctions plus a set of Lagrange multipliers which ensure normalization. This yields the complex scaled Kohn–Sham equations

$$H_{\mathrm{KS}}^\theta \psi_{\theta n}(\mathbf{r}) = \left[-\frac{1}{2}\mathrm{e}^{-i2\theta}\nabla^2 + v_\theta(\mathbf{r})\right]\psi_{\theta n}(\mathbf{r}) = \varepsilon_{\theta n}\psi_{\theta n}(\mathbf{r}) \tag{40}$$

for $\psi_{\theta n}(\mathbf{r})$ and $\varepsilon_{\theta n}$, where we have taken the derivative with respect to the left states $\overline{\psi}_{\theta n}(\mathbf{r})$. If the unscaled Hamiltonian is real, the states can be chosen to be real so that $\overline{\psi}_{\theta n}(\mathbf{r}) = \psi_{\theta n}(\mathbf{r})$. In general, however, we could equally well have derived a Hamiltonian for the left states $\overline{\psi}_{\theta n}(\mathbf{r})$.

In the Kohn–Sham equations (40) we have introduced the effective potential

$$v_\theta(\mathbf{r}) = v_{\mathrm{H}}^\theta(\mathbf{r}) + v_{\mathrm{xc}}^\theta(\mathbf{r}) + v_{\mathrm{ext}}\left(\mathbf{r}\mathrm{e}^{i\theta}\right) \tag{41}$$

defined as the density-derivatives of terms in the energy functional. The Hartree potential is

$$v_{\mathrm{H}}^\theta(\mathbf{r}) = \mathrm{e}^{-i\theta}\frac{\delta E_{\mathrm{H}}[\rho_\theta]}{\delta\rho_\theta(\mathbf{r})} = \mathrm{e}^{-i\theta}\int \frac{\rho_\theta(\mathbf{r}')}{\|\mathbf{r}' - \mathbf{r}\|}\mathrm{d}\mathbf{r}', \tag{42}$$

which allows the potential to be determined from the charge density by solving a complex Poisson problem using standard techniques. What remains to be discussed now is the XC functional.

4.2 Complex Scaling of Exchange and Correlation

The first DFRT calculations were carried out in a one-dimensional model potential with two electrons in the same (singlet) state [50]. The method was demonstrated using the exact KS potential, which in this case is

$$v^{\theta}_{\text{exact}}(x) = \mathrm{e}^{-i2\theta}\frac{\nabla^2\psi_\theta(x)}{2\psi_\theta(x)} + \varepsilon_\theta, \tag{43}$$

along with exact exchange (EXX) which, in this case, simply cancels out half the Coulomb energy. However, for systems with more particles, and indeed for realistic numerical calculations in the style of modern DFT software, the XC functional would have to be one of the many commonly used approximations. For simplicity we ignore any notion of spin below. The simplest functional is the local density approximation (LDA), the complex scaling of which was studied by Larsen et al. [49]. The first question is whether the functional is analytic. The exchange energy is given by

$$E_{\text{x}}[n] = -\frac{3}{4}\left(\frac{3}{\pi}\right)^{1/3}\int n^{4/3}(\mathbf{r})\mathrm{d}\mathbf{r}, \tag{44}$$

where the fractional power $n^{4/3}$ is three-valued on the complex numbers and we must mind the branch cuts. Following the arguments of Sect. 3.2 for handling the change in complex contour, the integral scales as follows as long as we do not run into a branch cut:

$$\begin{aligned}\int n^{4/3}(\mathbf{r})\mathrm{d}\mathbf{r} &= \int n^{4/3}\left(\mathbf{r}\mathrm{e}^{i\theta}\right)\mathrm{d}\mathbf{r}\mathrm{e}^{iN\theta} = \int \left[\mathrm{e}^{-iN\theta}n_\theta(\mathbf{r})\right]^{4/3}\mathrm{d}\mathbf{r}\mathrm{e}^{iN\theta}\\ &= \mathrm{e}^{-iN\theta/3}\int n_\theta^{4/3}(\mathbf{r})\mathrm{d}\mathbf{r}.\end{aligned} \tag{45}$$

The complex-scaled XC potential is naturally defined as

$$v^{\theta}_{\text{xc}}(\mathbf{r}) = \frac{\delta E^{\theta}_{\text{xc}}[n_\theta]}{\delta n_\theta(\mathbf{r})}. \tag{46}$$

Taking the derivative with respect to $n_\theta(\mathbf{r})$ we get the exchange potential

$$v^{\text{LDA}}_{\text{x}\theta}(\mathbf{r}) = -\left(\frac{3}{\pi}\right)^{1/3}\mathrm{e}^{-iN\theta/3}n_\theta^{1/3}(\mathbf{r}) = v^{\text{LDA}}_{\text{x}}\left(\mathbf{r}\mathrm{e}^{i\theta}\right), \tag{47}$$

i.e., the expression is consistent with analytically continuing the expression for the unscaled potential.

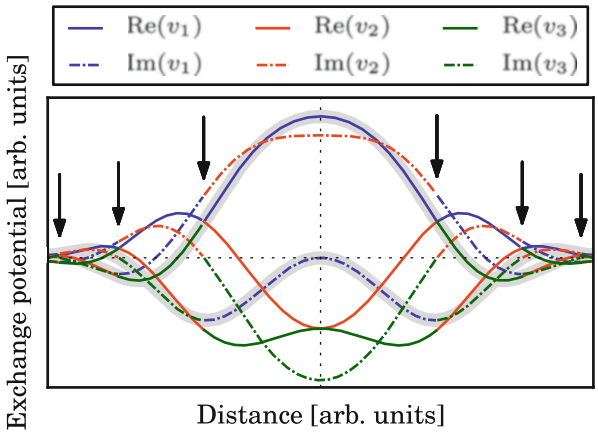

Fig. 6 "Stitching" branches of the cube root for the LDA exchange potential. The procedure starts at $x = 0$ where we know that the potential must be real. When the density takes the value of a branch cut of the cube root (indicated by *arrows*), the function must switch to a different branch to retain analyticity. The stitched function, indicated by the *shaded gray band*, is analytic everywhere and always follows one of the three branches of the cube root. In this example the density is a Gaussian function. From Larsen et al. [49]

As already noted, the expressions are three-valued because of the fractional power. In Larsen et al. [49] this was resolved by "stitching" the potential from the three branches of the cube root: In the origin, the potential must be real as the spatial co-ordinate is real. Further away, whenever the cube root encounters a branch cut, one of the other branches is chosen to restore analyticity. This procedure is illustrated in Fig. 6.

Following the Perdew–Wang parametrization of the LDA correlation functional [52], the correlation potential is given by

$$v_c(r_s) = \varepsilon_c(r_s) - \frac{1}{3}\frac{\mathrm{d}\varepsilon_c(r_s)}{\mathrm{d}r_s} r_s, \tag{48}$$

where

$$\varepsilon_c(r_s) = -2A(1 + \alpha_1 r_s)\ln(1 + 1/Q_1(r_s)), \tag{49}$$

$$Q_1(r_s) = 2A\sum_{i=1}^{4} \beta_i r_s^{i/2}, \tag{50}$$

and r_s is the Wigner–Seitz radius, i.e., $r_s(\mathbf{r}) = [3/(4\pi n(\mathbf{r}))]^{1/3}$. The complex logarithm can be stitched quite analogously to the cube root. Other XC functionals can be stitched similarly, provided that they do not contain poles that get in the way of the integration contour. With exterior complex scaling we avoid scaling the regions of space where most of the action happens, potentially avoiding these problems. We

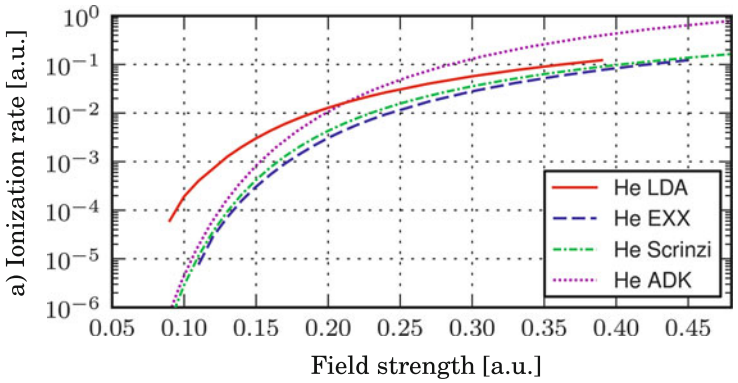

Fig. 7 Ionization rates of the helium atom in static electric fields from different methods. The accuracy at low field strengths is determined by how well the XC functional predicts the energy of the highest occupied orbital, which LDA is known to greatly overestimate. From Larsen et al. [49]

mention a recent time-dependent study [53] which uses smooth exterior complex scaling with the LB94 [54] XC model potential for spin σ:

$$v_{\mathrm{xc},\sigma}^{\mathrm{LB94}}(\mathbf{r}) = v_{\mathrm{xc},\sigma}^{\mathrm{LDA}}(\mathbf{r}) - \frac{\beta x_\sigma^2(\mathbf{r}) n_\sigma^{1/3}(\mathbf{r})}{1 + 3\beta x_\sigma(\mathbf{r}) \sinh^{-1} x_\sigma(\mathbf{r})} \tag{51}$$

with

$$x_\sigma(\mathbf{r}) = \frac{\|\nabla n_\sigma(\mathbf{r})\|}{n_\sigma^{4/3}(\mathbf{r})}. \tag{52}$$

This expression also has several issues with analyticity as it involves both division and fractional powers. In Telnov et al. [53] the exterior scaling contour was probably chosen so as to avoid these, but unfortunately the issue was not mentioned.

4.3 Resonance Lifetimes in DFRT

In this section we present a few results from DFRT on physical systems. Figure 7 shows the ionization rate of a helium atom in an electric field as a function of field strength calculated with different methods: LDA, EXX (Hartree–Fock), ADK [55], and an accurate correlated-electron calculation by Scrinzi [45].

ADK is a simple approximation which is correct in the limit of weak fields. The ionization potential of the atom entirely determines the form of the curve in this limit. Precisely because low-field asymptotics are determined by the value of the ionization potential, the utility of a functional in this limit is directly linked to the

precision with which it estimates the ionization potential, i.e., which energy it assigns to the highest occupied state.

LDA is well known to overestimate this energy, and therefore calculates too high ionization rates for low fields. This problem is attributed to the wrong asymptotic decay of the LDA potential [54]. Meanwhile, Hartree–Fock is known to produce accurate orbital energies, and the decay of the exact exchange potential has the correct asymptotic form. EXX also yields results that are close to the reference by Scrinzi. This all suggests that a good XC functional for DFRT resonance lifetime calculations is one retaining the correct asymptotic form of the potential, such as the previously mentioned LB94 functional.

4.4 Time-Dependence in Complex Scaling

In this section we consider the extension of complex scaling to time-dependent simulations. Most obviously, one could simulate the dynamics of a system whose initial state is derived from a resonance. However, the method has been found useful for another practical reason, namely that complex scaling can be used to avoid the effects of waves reflecting from the boundaries. An early approach by Parker and McCurdy [56] showed that a complex basis set, with properties closely related to the complex scaling method, reduced the amount of basis functions necessary to represent properly a Gaussian wave packet under time evolution. The authors found that the representation avoided reflection effects produced by incompleteness of the basis sets as the wave packet moved away from the central region.

Exterior complex scaling is now widely used as a practical absorber to prevent reflections of waves because of the finite size of the simulation box. Details of its use in this context are given in Sect. 5.6.

Let us go back to the basic question of how to time evolve complex-scaled states. Bengtsson and co-workers [57, 58] have considered this problem in detail. The time evolution of a state vector and its corresponding functional (or bra) are determined by

$$i\frac{\partial\psi(\mathbf{r}t)}{\partial t} = \hat{H}\,\psi(\mathbf{r}t). \tag{53}$$

We apply the complex rotation operator and get

$$i\frac{\partial\psi_\theta(\mathbf{r}t)}{\partial t} = i\hat{R}_\theta\frac{\partial\psi(\mathbf{r}t)}{\partial t} = \hat{R}_\theta\hat{H}\hat{R}_\theta^{-1}\hat{R}_\theta\psi(\mathbf{r}t) = \hat{H}_\theta\psi_\theta(\mathbf{r}t). \tag{54}$$

A general state $\psi_\theta(\mathbf{r}t)$ can be time-evolved according to its expansion in eigenstates. If $\phi_\theta^0(\mathbf{r})$ is an eigenstate with energy ε_θ, then

$$\phi_\theta(\mathbf{r}t) = \mathrm{e}^{-i\hat{H}_\theta t}\phi^0_\theta(\mathbf{r}) = \mathrm{e}^{-i\epsilon_\theta t}\phi^0_\theta(\mathbf{r}). \tag{55}$$

If, further, the eigenstate represents a resonance, so that its energy has a negative imaginary part, $\phi_\theta(\mathbf{r}t)$ decays exponentially while everywhere maintaining its shape. To calculate a general expectation value after a certain time, we would, according to (10), need to apply the *left* state $\overline{\psi}_\theta(\mathbf{r}t) = [\psi_{-\theta}(\mathbf{r}t)]^*$ as per (12). The left state can be time evolved using (54) with $-\theta$. The Hamiltonian $\hat{H}_{-\theta}$ is the conjugate of $\hat{H}_\theta$ so all eigenvalues are likewise conjugated. If $\psi_\theta(\mathbf{r}t)$ contains exponentially decaying components, the corresponding components of $\psi_{-\theta}(\mathbf{r}t)$ exponentially increase at the same rate (one could equivalently say that they propagate backward in time [59]). In principle the increase of the left state would be cancelled by the decay of the right so that the norm, calculated using both left and right states, is time independent, but any numerical error accumulates over the course of the time evolution and eventually causes the procedure to break down.

Although Bengtsson and co-workers have demonstrated that a complex time propagation path can be used to stabilize the time evolution [58], most applications of complex scaling with time evolution have been handled differently. The typical approach is to use exterior complex scaling and time evolve only the right states, then calculate all physical quantities using only the right states although this in general is not formally justified. This approach is discussed further in Sect. 5.6.

5 Open Boundary Conditions

In the previous sections we showed how it is possible to capture intrinsically time-dependent properties such as the lifetime of a resonance using a static, time-independent approach. Now we turn instead to the class of problems where the explicit time-dependence must be taken into account. As we see, the concepts introduced in the previous sections reemerge in the description of physical processes where the total number of particles is no longer a conserved quantity. In particular, insistence on describing an infinitely extended problem in a bounded domain naturally results in dynamics governed by a non-Hermitian Hamiltonian.

Let us divide space into two parts as in Fig. 8 where we have a bounded region we call A and its complement B. We want to solve the equations of motion in A without having to describe explicitly the environment in B. In other words, the problem we have is finding the appropriate boundary conditions for the equations in A, such that the localized solution $\Psi_A(t)$ is equal to the full solution $\Psi(t)$ evaluated in A at all times t.

The class of processes which can be described by the scheme in Fig. 8 includes all the scattering problems where electrons enter A from one side and escape after having interacted with the system. This encompasses, for instance, electron diffraction or molecular transport. It also includes scattering problems where electrons are scattered by other kinds of particles such as photons or protons, thus leading to

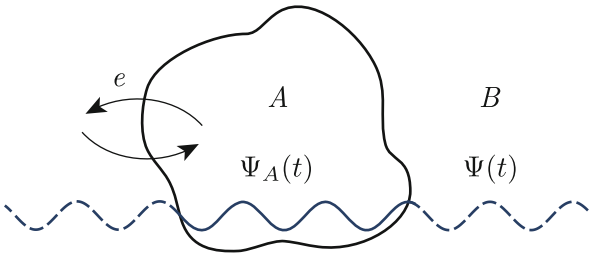

Fig. 8 A system localized in a bounded region A exchanges electrons with the environment B. We look for the correct boundary conditions for the TDSE in A such that the bounded wavefunction $\Psi_A(t)$ matches the complete wavefunction $\Psi(t)$ at all times t

photoionization or proton impact ionization. This last class of processes is sometimes called half-scattering processes because, from the point of view of the electron, the scattering happens with another kind of particle. The main difference between scattering and half-scattering processes is that the boundary conditions for describing the half process are simpler because there is no need to inject charge but only to absorb it. We must, however, note that if nonlinear effects are dominant, for instance when strong laser fields are involved, this distinction is less clear and one may also need to account for incoming electrons for half-scattering problems.

Below we review some of the most notable methods in the literature that have been employed to address this problem. We anticipate that, in all the approaches we discuss, the boundary conditions are implemented by modifying the Hamiltonian with the addition of a complex term that explicitly breaks Hermiticity.

5.1 *Transparent Boundary Conditions Using Green Functions*

Transparent boundary conditions include, by definition, all boundary conditions that allow an exact solution of the open boundary problem. As such, they allow electrons to move back and forth between A and B without reflection. We examine below the class of boundary conditions that can be defined in terms of Green functions. This is not the only possible solution, and other instances of transparent boundaries can be constructed, for example, by using *time dependent exterior complex scaling* or *split propagation schemes* as we show in Sects. 5.6 and 6.3, respectively. So-called *decimation* techniques have also been employed to describe transparent boundaries; see, for instance, García-Moliner and Flores [60] and Kudrnovský et al. [61].

Green function boundary conditions are based on the idea of matching the inner solution Ψ_A of the Schrödinger equation with the outer one Ψ_B expressed in terms of Green functions. Underlying this strategy is the hypothesis that the Hamiltonian describing the system in B is easier to handle than the one describing the system in A.

In general, the problem of finding the Green function for an arbitrary system is hard to solve. However, including in A most of the atomic and molecular structure leaves us in B with a problem which, in many cases, can be easily solved.

The simplest case consists of choosing B to represent the empty space, and the method lends itself to the description of scattering or ionization [62, 63]. On a more advanced level, one may choose B to represent a bulk system and, in conjunction with a time-dependent potential, create a base model for electron transport [64, 65]. Alternatively, by mixing both bulk and empty space Green functions, the frameworks can adapt to the description of ionization from surfaces [66, 67].

The approach is adaptable to a large variety of situations. This versatility has, however, to face the fact that discretizing the otherwise exact equations often leads to computationally demanding implementations with limited application. On the practical level, either one introduces an approximation which affects the quality of the results, or one just uses a simple time propagation of a full-dimensional system, which represents a challenging task [68].

In spite of the technical limitations, the approach provides a fundamental and illustrative description of the open boundary problem. Below we discuss two of the most notable derivations present in the literature.

5.2 Time-Dependent Embedding

The original Green function embedding was developed in the context of surface and solid state physics for the static Schrödinger equation by Inglesfield [69]. It was subsequently extended to the time-dependent case in Inglesfield [67, 70] by the same author, but similar derivations have been proposed earlier in different fields, for instance, to describe the interaction of a strong laser with atoms in Boucke et al. [62] and Ermolaev et al. [63], and for electron transport in Hellums and Frensley [64].

Below we introduce the theory following an approach similar to the one used to describe molecular transport with TDDFT by Kurth [65].[4] We first restrict ourselves to the single-electron case and then discuss the extension to the many-electron one with TDDFT.

Let us consider the case of a system in contact with a reservoir as shown in Fig. 9. We want to find a closed set of conditions that have to be imposed on the equations for a wavefunction in A such that it correctly matches its outer part in B for all times. Following the division in the figure, we can write the time-dependent Schrödinger equation for the system A coupled with a reservoir/environment B using a block matrix representation:

[4] An analogous approach was first presented by Hellums [64] in a single-particle picture.

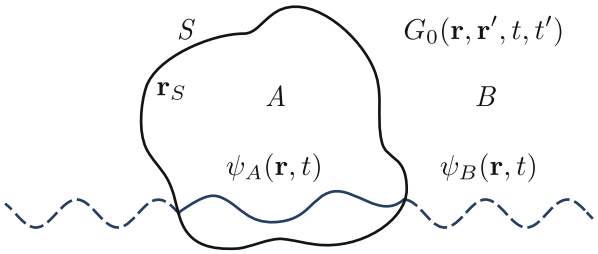

Fig. 9 Time-dependent embedding. Embedding consists in modifying the Hamiltonian in A in such a way that, solving the associated time-dependent Schrödinger equation in A only, it automatically imposes the matching of $\psi_A(\mathbf{r},t)$ with $\psi_B(\mathbf{r},t)$ for all t. The modification is made using an embedding operator derived in terms of the Green function $G_0(\mathbf{r},\mathbf{r}',t,t')$ of the environment B

$$i\frac{\partial}{\partial t}\begin{bmatrix}\psi_A(\mathbf{r},t)\\ \psi_B(\mathbf{r},t)\end{bmatrix} = \begin{bmatrix}\hat{H}_{A,A}(t)\hat{H}_{A,B}(t)\\ \hat{H}_{B,A}(t)\hat{H}_{B,B}(t)\end{bmatrix}\begin{bmatrix}\psi_A(\mathbf{r},t)\\ \psi_B(\mathbf{r},t)\end{bmatrix}, \tag{56}$$

where $\psi_A(\mathbf{r},t)$ and $\psi_B(\mathbf{r},t)$ are the wavefunctions projected onto each separate region. Here we consider the general case where the Hamiltonian is time-dependent, and its components include two diagonal terms $\hat{H}_{A,A}(t)$ and $\hat{H}_{B,B}(t)$ operating within each separate region and two coupling terms $\hat{H}_{A,B}(t)$ and $\hat{H}_{B,A}(t)$ connecting the environment to the system.

To derive the embedded time-dependent equations we introduce the retarded Green function G_0 for the reservoir, defined as

$$\left[i\frac{\partial}{\partial t} - \hat{H}_{B,B}(t)\right]G_0(\mathbf{r},\mathbf{r}',t,t') = \delta(\mathbf{r}-\mathbf{r}')\delta(t-t'), \tag{57}$$

with boundary conditions $G_0(\mathbf{r},\mathbf{r}',t^+,t) = -i$, $G_0(\mathbf{r},\mathbf{r}',t,t^+) = 0$, and where t^+ represents a time approaching t from above. Because of the explicit time dependence of $\hat{H}_{B,B}(t)$, it generally depends on both the time variables t and t'. We note however that the solution greatly simplifies if we consider B to represent empty space. In this case, $G_0(\mathbf{r},\mathbf{r}',t,t')$ is the free propagator, which depends only on the time difference $t-t'$ and is known analytically.

Using $G_0(\mathbf{r},\mathbf{r}',t,t')$ we can directly build the solution of the differential equations in B. This corresponds to considering only the second row in (56), and results in[5]

[5] To simplify notation we avoid explicitly writing out all the coordinates. We also use the same convention used in Kurth et al. [65] where operators are thought of as matrices with continuous indices along the spatial coordinates. We thus omit explicit reference to $\mathbf{r}$ and $\mathbf{r}'$ and interpret operator products as integrals.

$$\psi_B(t) = iG_0(t,0)\psi_B(0) + \int_0^t \hat{G}_0(t,t')\hat{H}_{B,A}(t)\psi_A(t')\mathrm{d}t'. \tag{58}$$

The final equation governing the time evolution for $\psi_A(t)$ can be written in a closed form simply by plugging (58) into the first row of (56). After that we obtain

$$i\frac{\partial \psi_A(t)}{\partial t} = \hat{H}_{A,A}(t)\psi_A(t) + \hat{H}_\Sigma[\psi_A](t) \tag{59}$$

with

$$\hat{H}_\Sigma[\psi_A](t) = \int_0^t \hat{\Sigma}(t,t')\psi_A(t')\mathrm{d}t' + i\hat{H}_{A,B}(t)\hat{G}_0(t,0)\psi_B(0). \tag{60}$$

In this equation, $\hat{\Sigma}(t,t') = \hat{H}_{A,B}(t)\hat{G}_0(t,t')\hat{H}_{B,A}(t')$ can be identified with the self-energy responsible for the hopping in and out of the system, whereas the last term is responsible for imposing the initial conditions in the reservoir. It is zero if the wavefunction is completely localized in A at $t=0$. The time evolution of $\psi_A(t)$ is thus governed by a modified Hamiltonian containing an additional time-dependent embedding operator $\hat{H}_\Sigma[\psi_A](t)$. The dependence on the wavefunction is written in square brackets to stress the fact that $\hat{H}_\Sigma[\psi_A](t)$ is not just a simple local potential but involves a more general non-local action.

The kernel $\hat{\Sigma}(t,t')$ of the time integral in (60) is, in the most general case, an explicit function of t and t'. This is the case, for instance, when one wants to apply this method to model molecular transport and B represents an electrode with a time-dependent voltage bias. Evaluating (60) thus requires one to keep track of $\psi_A(t)$ for all times up to t. This is one of the biggest drawbacks of the approach as it restricts the propagation to short times because of storage limitations. Direct approximations of the kernel intended to mitigate this problem have to face the fact that the kernel is often non-analytical and highly oscillating, especially for $t \to t'$ [65]. However, we note that when the Hamiltonian in B is not explicitly time-dependent, $\hat{\Sigma}(t,t')$ depends only on the time difference $t-t'$ and we are left with a much easier convolution integral.

In this last case, i.e., when the Hamiltonian in B is time-independent, an alternative but equivalent form for the embedding operator can be obtained following the derivation of Inglesfield [67]. In this approach we are given two wavefunctions $\psi_A(\mathbf{r},t)$ and $\psi_B(\mathbf{r},t)$ which have equal amplitude on the surface S separating A and B, but arbitrary derivative as illustrated in Fig. 9. Assuming that $\psi_B(\mathbf{r},t)$ is a solution of the time-dependent Schrödinger equation in B, we need to find a closed set of equations for $\psi_A(\mathbf{r},t)$ to connect perfectly to $\psi_B(\mathbf{r},t)$ on S for all t.

The problem is solved with the use of what in the field of partial differential equations goes under the name of Dirichlet-to-Neumann and its inverse Neumann-to-Dirichlet maps [68, 71, 72]. These maps allow one to transform Dirichlet

boundary conditions, fixing the value of a function on a surface, into Neumann boundary conditions, fixing the normal derivative over a surface, and vice versa. The resulting time-dependent equations for $\psi_A(\mathbf{r},t)$ can be written in the same way as (59) with an embedding operator defined as [67, 70]

$$\hat{H}_{\mathcal{E}}[\psi_A](t) = \delta(\mathbf{r}-\mathbf{r}_S)\left[\frac{1}{2}\frac{\partial\psi_A(\mathbf{r}_S,t)}{\partial n_S} + \int_S\int_0^t \overline{G}_0^{-1}(\mathbf{r}_S,\mathbf{r}'_S,t-t')\frac{\partial\psi_A(\mathbf{r}'_S,t')}{\partial t'}\mathrm{d}t'\mathrm{d}\mathbf{r}'_S\right], \tag{61}$$

where $\partial/\partial n_s$ denotes the directional derivative out of A and perpendicular to S, and

$$\overline{G}_0^{-1}(\mathbf{r}_S,\mathbf{r}'_S,t) = \frac{1}{2\pi}\int_{-\infty}^{\infty} \mathrm{e}^{-i\varepsilon t}G_0^{-1}(\mathbf{r}_S,\mathbf{r}'_S,\varepsilon)\mathrm{d}\varepsilon. \tag{62}$$

Here $G_0^{-1}(\mathbf{r}_S,\mathbf{r}'_S,\varepsilon)$ is the inverse of the Green function defined by (57) evaluated on the boundary surface S with $\mathbf{r}_S,\mathbf{r}'_S \in S$. Because $G_0(\mathbf{r},\mathbf{r}',t-t')$ depends only on time differences it is conveniently expressed in the energy domain ε with a Fourier transform over the time domain. Because of the presence of the $\delta(\mathbf{r}-\mathbf{r}_S)$, the embedding operator (61) is non-zero only on the boundary surface and involves normal and time derivatives of $\psi_A(\mathbf{r},t)$ over that surface.

Because of the equivalence of $\hat{H}_{\mathcal{E}}$ and $\hat{H}_{\Sigma}$ defined in (60) and (61), we refer in the following to an embedding operator with the symbol $\hat{\mathcal{E}}[\psi_A](t)$ for simplicity. We are now in the position to comment on the most characteristic features of $\hat{\mathcal{E}}[\psi_A](t)$. In general, it involves complex quantities which make it an explicitly non-Hermitian operator. This fact implies that the total number of electrons is no longer conserved during the propagation. Furthermore, it contains a memory term in the form of a time integral. In Frensley [73] it was postulated that transparent boundary conditions should break time reversal symmetry. The presence of a memory term in (59) turns the time propagation into a non-Markovian process and precisely breaks this symmetry.

The extension to the many-electron case is straightforward using the same 2×2 block structure of (56) with the difference that the entries must be interpreted as operators acting on the N-body Hilbert space. The previous steps of the derivation hold in a completely equivalent way up to (59) and (60) provided the interacting many-body Green function G is used in place of G_0.

Formulating this in the language of TDDFT, the OQS-TDDFT theory establishes a one-to-one connection between potential and density for non-unitary dynamics [5–7]. The evolution from an initial state is uniquely defined if we find a way to write the coupling with the environment as a functional $\nu^B[n]$ of the total density n. Once again the equations retain the block structure of (56) with entries interpreted as multi-index tensors, each index being associated with a Kohn–Sham orbital. The result is a set of equations equivalent to (59) for each orbital, where the exact embedding operator $\hat{\mathcal{E}}[n]$ depends on the total density of the system (i.e., in $A\cup B$)

through each orbital and the full many-body Green function $G[n]$. The total embedding operator can thus be interpreted as the coupling functional $\nu^B[n]$ with the environment. Obviously, this connection involving the full many-body Green function is of little use in practical situations, but it provides a clear starting point for further approximations.

5.3 Absorbing Boundaries

Describing charge transfer between a system and its environment implies a modification of the isolated Hamiltonian. In the previous section we showed how the exact condition requires the addition of an embedding operator $\hat{\mathcal{E}}[\psi_A](t)$ that turns the Hamiltonian non-Hermitian. The evaluation of such an operator can, however, be very demanding and one needs to resort to simpler strategies.

Absorbing boundaries (ABs) or boundary absorbers are cheaper options. They can be defined as any approximation of the form

$$\hat{H}_{\mathrm{AB}}[\psi_A(t)](t) \approx \hat{\mathcal{E}}[\psi_A](t) \tag{63}$$

to an embedding operator such as the one given by (60) or (61). This approximation is specific to the case where B represents the empty space and we only have to absorb outgoing electrons. We know that $\hat{\mathcal{E}}[\psi_A](t)$ can be spatially localized on the boundary surface. The absorbing boundary operator is instead generally allowed to act on the wavefunctions over a larger region close to the boundaries, as illustrated in Fig. 10. In the large majority of approximations, this operator is taken to be a local potential:

$$\hat{H}_{\mathrm{AB}}[\psi_A(t)](t) = \hat{V}_{\mathrm{AB}}(t)\psi_A(t). \tag{64}$$

Its purpose is to absorb completely any outgoing wave packet entering the region (striped in the figure) of its support. The main goal here is to apply the absorber that best simulates the exact embedding operator with the minimum computational cost.

From a TDDFT perspective, when we apply $\hat{H}_{\mathrm{AB}}$ to each Kohn–Sham orbital, on top of all the approximations which might be involved in the description of the embedding operator, we are also approximating the interaction between the system and the environment by setting it to zero.

The absorbing properties of a boundary depend strongly on the numerical implementation. We do not enter any specific implementation here but just point out the fact that none of the absorbers presented in the literature are completely free from reflections. We refer to De Giovannini et al. [74] for a recent review on the reflection properties of members of each boundary family.

We discuss below two of the most popular families of absorbing boundaries: the complex absorbing potentials (CAPs) and the mask function absorbers (MFAs).

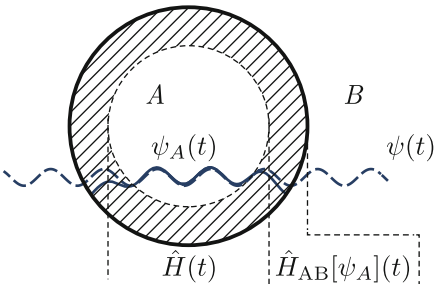

Fig. 10 Absorbing boundaries. An absorbing boundary Hamiltonian $\hat{H}_{\mathrm{AB}}(t)$ acting on the striped region is added to the original one $\hat{H}(t)$ to prevent reflections from the boundaries during time propagation. The perfect absorber is the one that matches the full solution $\psi(t)$ with $\psi_A(t)$ in the inner (*non-striped*) region for all times t

These families are substantially phenomenological approximations to the open boundary problem for which the main point of attraction rests on their simplicity of implementation and limited computational costs.

5.4 Complex Absorbing Potentials (CAPs)

We already noted above that the exact embedding potential has to be a complex quantity to turn the Hamiltonian non-Hermitian, and the fundamental mechanism of CAPs is precisely based on this observation. The idea was originally introduced from a different standpoint by Neuhauser and Baer [75, 76] with the use of negative imaginary potentials for the Schrödinger equation. This was in connection with the so-called optical potentials or perfectly matched layers developed for electromagnetic waves [77].

The effect of a CAP can be easily understood by observing the action of the infinitesimal time evolution operator on a wavefunction

$$\hat{U}(t + \mathrm{d}t, t)\psi_A(t) = \exp\left[-i\left(\hat{H}(t) + \hat{V}_{\mathrm{CAP}}\right)\mathrm{d}t\right]\psi_A(t), \tag{65}$$

when $\hat{V}_{\mathrm{CAP}}$ is a negative imaginary potential with support on a region close to the boundaries of A. In this case, the effect simply results in an exponential suppression of the wavefunction in the absorbing region. In other words, the time evolution operator associated with the non-Hermitian Hamiltonian modified with $\hat{V}_{\mathrm{CAP}}$ is non-unitary and no longer conserves the wavefunction norm. The norm decreases if $\hat{V}_{\mathrm{CAP}}$ is negative and increases if it is positive. In the latter case it becomes possible to simulate charge injection, and this fact has been used to mimic reservoirs acting as sinks or sources in the attempt to simulate electron transport [78–80].

CAPs are by no means restricted to purely imaginary potentials and there is a huge body of literature describing their different forms and declinations [81]. We

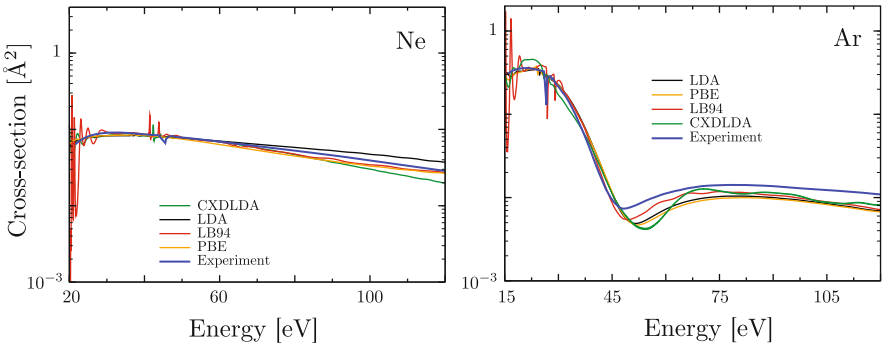

Fig. 11 Neon and argon atom absorption cross-sections above the first ionization threshold calculated with TDDFT and different exchange and correlation functionals: LDA, CXD-LDA [82], PBE [83], and LB94 [54]. A CAP is introduced to reduce reflections in an energy window centered around $E = 93$ eV (Ne) and $E = 105$ eV (Ar). Adapted from Crawford-Uranga et al. [84]

stress the fact that their properties strongly depend both on their mathematical form and the specific implementation, and, without exception, they all reflect in some energy range [74]. For practical purposes it is thus very important to ensure that the CAP we choose for our calculations has good absorption properties in the range of interest.

As an example, in Fig. 11 we show the absorption cross-sections for argon and neon in the continuum, above the first ionization threshold, calculated in linear response with TDDFT and a CAP. The CAP is chosen to minimize reflections around $E = 93$ eV for neon and $E = 105$ eV for argon. The spectra are in good agreement with the experimental ones in a fairly large range around those energies and reflections appear as oscillations.

What is interesting about this result is that we are able to calculate a quantity involving transitions to infinitely extended continuum states just performing a time propagation in a bounded volume. Although at first it might seem counterintuitive, the explanation is actually quite intuitive. In fact, we are calculating here a quantity involving the dipole matrix element between an initial state, the ground state of our system Ψ_0, to a final state, a continuum state $\Psi_{E>0} : \langle \Psi_0 | \hat{d} | \Psi_{E>0} \rangle$. The main contribution to this matrix element comes from an integration over the overlap region between the two wavefunctions and, because the ground state is bounded, this region is safely included in A. The extent to which we manage to remove reflection thus directly relates to the quality with which we calculate this integral and, eventually, the quality of the absorption cross-section.

5.5 Mask Function Absorbers (MFAs)

MFAs are an alternative formulation of CAPs. They have been employed to study a variety of phenomena including high harmonic generation [85], electron and proton emission [86], and above-threshold ionization [87].

They are defined by directly modifying the infinitesimal time evolution operator with a mask function $M(\mathbf{r})$ as follows:

$$\hat{U}_{\mathrm{M}}(t + \mathrm{d}t, t) = \mathrm{M}(\mathbf{r})\hat{U}(t + \mathrm{d}t, t). \tag{66}$$

The effect of this modification can be easily understood by choosing $M(\mathbf{r})$ to be a real function equal to 1 in the inner part of A and smoothly decaying to zero close to the boundaries. With this choice, recursive application of $U_{\mathrm{M}}(t+\mathrm{d}t,t)$ to $\psi_A(t)$ directly suppresses the part of the wavefunction in the decay region.

This is only one of the possible choices of MFA and, in general, $M(\mathbf{r})$ can be a complex function. We illustrate the effect of using complex $M(\mathbf{r})$ by showing the equivalence between MFAs and CAPs. In fact, given a $\hat{V}_{\mathrm{CAP}}$, we can obtain the corresponding $M_{\mathrm{CAP}}(\mathbf{r})$ straightforwardly by expanding the exponential in (65). To first order in dt the MFA $M^{(1)}_{\mathrm{CAP}}$ associated with $\hat{V}_{\mathrm{CAP}}$ is

$$M^{(1)}_{\mathrm{CAP}}(\mathbf{r}) = \mathrm{e}^{-iV_{\mathrm{CAP}}(\mathbf{r})\mathrm{d}t}. \tag{67}$$

The mask function can thus be a complex function, and becomes real when $\hat{V}_{\mathrm{CAP}}$ is purely imaginary. The inverse relation can be obtained in a similar way, and to first order it reduces to

$$V^{(1)}_{\mathrm{MFA}}(\mathbf{r}) = \frac{i}{\mathrm{d}t}\ln[M(\mathbf{r})]. \tag{68}$$

In De Giovannini et al. [74] it was shown that the first-order relations above, for a given pair of CAP and MFA, yield reflection properties in excellent agreement with each other.

One important feature of the MFA approach is that by multiplying $M(\mathbf{r})$ and $1 - M(\mathbf{r})$ by a wavefunction it is possible to split its propagation in two different components moving in separate regions. This property is fundamental for split-domain propagation schemes initially derived in Chelkowski et al. [88] and Grobe et al. [89] and later extended to the study of electron photoemission with TDDFT in De Giovannini et al. [90]. We return to this point in Sect. 6.3.

5.6 Time-Dependent Exterior Complex Scaling

In Sect. 3.5 we introduced *exterior complex scaling* as an extension of *complex scaling* where the transformation is only applied outside a certain region. It was noted that it shares an important feature with the global transformation: it naturally imposes outgoing boundary conditions on the Schrödinger equation. We discuss here to what extent this property applies to the time-dependent case.

Let us consider a scaling transformation similar to those illustrated in Fig. 3. We further select a path on the real axis deep into region A that departs for the complex plane at some point close to the boundary and eventually reaches the asymptotic form $\mathbf{r} \to \mathbf{r}e^{i\theta}$. Following this scaling transformation, the time-dependent Schrödinger equation can be formally cast into a set of equations:

$$i\frac{\partial \psi_\theta(\mathbf{r},t)}{\partial t} = \hat{H}_\theta^{\mathrm{ECS}}(t)\psi_\theta(\mathbf{r},t) \tag{69}$$

$$-i\frac{\partial \overline{\psi}_\theta(\mathbf{r},t)}{\partial t} = \hat{H}_\theta^{\mathrm{ECS}}(t)\overline{\psi}_\theta(\mathbf{r},t). \tag{70}$$

for left $\overline{\psi}_\theta(\mathbf{r},t)$ and right states $\psi_\theta(\mathbf{r},t)$, where $\hat{H}_\theta^{\mathrm{ECS}}(t)$ represents the scaled Hamiltonian. Extrapolating from the discussion in Sect. 4.4 we can interpret (69) as imposing purely outgoing boundary conditions and (70) as the incoming counterpart.

In the theory of *complex scaling*, the calculation of the expectation value of an observable $\hat{O}_\theta$ on the scaled path as of (10) involves left and right states on an equal footing. This extends to the time-dependent case with the requirement of having both left and right states at the same time to calculate $\hat{O}_\theta$. Hence, we need, in principle, to solve (69) and (70) simultaneously.

The fact that the scaling path lies exactly on the real axis in a certain region simplifies the equations. In fact, on the real axis, left and right states are complex conjugates: $\overline{\psi}_\theta(\mathbf{r},t) \equiv [\psi_{-\theta}(\mathbf{r},t)]^* = \psi_\theta(\mathbf{r},t)^*$ for $\mathbf{r}$ in the interior region. This is particularly true when the system contains only a local potential and the propagation is initialized with a state localized in the unscaled region at $t=0$ and propagating outward. If we restrict ourselves to observables in the unscaled region and we want to describe a purely outgoing process, we resolve to use the right state $\psi_\theta(\mathbf{r},t)$ only. This state can be obtained by propagating (69) which involves only right states [38]. Following this, most applications of *exterior complex scaling* are limited to a use with the decaying right states and observables evaluated in the unscaled region.

Equation (69) perfectly describes problems where imposing purely outgoing boundary conditions represents an exact condition similar to that, for example, in ionization processes. In those cases it can be regarded as equivalent to a transparent boundary condition described with a Green function. Here, because we are dealing with purely outgoing conditions, we should note that the title of perfect absorber is

more appropriate than that of transparent boundary, because electrons can flow in only one direction.

However, we note an important difference between the two approaches. Whereas the Green function embedding defines the exact matching conditions at the boundary of a finite volume A, the scaled (69) acts on a wavefunction defined in the full space $A \cup B$. This makes the size of the simulation box a weakness in numerical simulations if a wave is capable of reaching the end of the box. The scaling transformation imposes an asymptotic form which can be efficiently captured by exponential functions $e^{-\alpha r}$. By employing a finite element approach with an element at infinity which captures the exponential tail, it was numerically shown by Scrinzi [38] that *exterior complex scaling* indeed provides perfectly absorbing conditions for numerical precision.

Restricting (69) to A otherwise implies a truncation which irrevocably breaks its perfect properties. In this case the scaling transformation reduces to an absorbing boundary which can be regarded as a simple CAP and, as such, presents reflections [74, 91]. We should mention that the use of (69) restricted to A in combination with a *smooth exterior complex scaling* in the literature has been going under the misleading name of reflection-free CAP, in spite of presenting a certain degree of reflection [39, 91–93].

In the context of TDDFT, *exterior complex scaling* has been applied purely as an absorbing boundary [53, 94].

6 Electron Photoemission

We focus here on the approaches that can be employed in the description of multi-electron ionization initiated by external electromagnetic fields within TDDFT. As in previous sections, we are interested only in electronic processes, neglecting any ionic motion, and we restrict ourselves to the class of methods that requires knowledge of the wavefunctions only on a bounded region of space A much as in Fig. 8.

We are interested in the family of problems characterized by time-dependent electronic Hamiltonians with the structure

$$\hat{H}(t) = \frac{1}{2}\left[-i\nabla - \frac{\boldsymbol{\mathcal{A}}(t)}{c}\right]^2 + v_{\text{ext}} + v_{\text{ee}}, \tag{71}$$

where v_{ee} is the electron–electron Coulomb interaction, v_{ext} is the external potential which generally consists of a static potential produced by the nuclei, $\boldsymbol{\mathcal{A}}(t)$ is the vector potential of the external field, and c is the speed of light. In writing (71) we implied the choice of the velocity gauge to describe the action of the field. The associated electric field can easily be obtained as a time derivative: $\boldsymbol{\mathcal{E}}(t) = -\partial_t \boldsymbol{\mathcal{A}}(t)$. Typically, one would want to perform a simulation by choosing

a vector potential representing one or more laser pulses, then investigate the induced dynamic.

Ionization takes place whenever the field is capable of inducing a bound-to-continuum transition, resulting in electrons escaping with a given kinetic energy. Calculation of observables characterizing these ionized electrons is at the center of our interest here.

To some extent we already approached this problem in Sect. 5. In fact, total ionization can be naturally described using only information contained in a bounded volume A surrounding our system. The total number of electrons contained in A can be simply calculated from the knowledge of the time-dependent density as

$$N(t) = \int_A n(\mathbf{r}, t) \mathrm{d}\mathbf{r}. \tag{72}$$

Combined with the use of one of the boundary conditions described above, (72) implements a practical strategy for the calculation of $N(t)$. The total ionization probability, i.e., the probability of ejecting an electron in the long-time limit, is thus naturally obtained using only quantities defined in A as

$$\mathcal{P} = \lim_{t\to\infty} \frac{N - N(t)}{N}, \tag{73}$$

where N represents the total number of electrons in the system before ionization. Being a direct functional of the density, $\mathcal{P}$ is an exact quantity within TDDFT and does not present any further approximation besides the one involved with the use of the boundary conditions.

In many situations the quantities containing relevant physical information are more complex objects than the simple total ionization probability, and one would wish to access differential probabilities with respect to energy or momentum:

$$P(E) = \frac{\partial \mathcal{P}}{\partial E}, \quad P(\mathbf{k}) = \frac{\partial^3 \mathcal{P}}{\partial k_x \partial k_y \partial k_z}. \tag{74}$$

The calculation of these observables within TDDFT is, however, not as straightforward as the evaluation of $\mathcal{P}$.

The first reason is the intrinsic complexity of the ionization process already with only one electron. There are situations, especially when strong laser fields are involved, where the electron dynamics are so complex that one has to propagate explicitly the wavefunction in time to account for the process. In principle, the differential probabilities can then be obtained by projecting the scattering wavefunction $\Psi_s(t)$ onto the appropriate set of scattering wavefunctions ϕ_E as

$$P(E) = \lim_{t\to\infty} \left|\left\langle \phi_E \middle| \Psi_s(t) \right\rangle\right|^2 \quad \text{with } E > 0. \tag{75}$$

Besides the issues related to the correct evaluation of the projecting set, owing to their large spatial extension, the propagation of the total electronic wavefunction at long times can be practically performed only for highly symmetrical systems, such as atoms and small molecules, or for short times. Alternative approaches, such as those we describe below, involve the knowledge of the wavefunction only in a bounded region of space.

The second reason has to do with the multi-electron nature of ionization at the TDDFT level. In fact, whereas the connection between $\mathcal{P}$ and the total density is explicitly known, the differential quantities (74) cannot be easily expressed in terms of the density. The derivation and the use of appropriate density functionals to describe $P(E)$ and $P(\mathbf{k})$ from (74) are thus important and have to take into account in our model.

In the following we discuss the methods that have been developed to tackle these problems numerically.

6.1 Sampling Point Method

A simple scheme to evaluate the energy-resolved photoelectron distribution $P(E)$ was proposed by Pohl et al. [95]. Lacking clear theoretical foundations, this method has some limitations to its range of applicability. We briefly review it here for historical reasons connected to the fact that, together with the mask method of Sect. 6.3, it is the only method that has been employed to calculate $P(E)$ from (74) for molecular systems with TDDFT.

The method consists in recording the time evolution of each Kohn–Sham orbital $\psi_i(\mathbf{r}_S,t)$ at given points in space $\mathbf{r}_S$ as shown in Fig. 12. This time evolution is then turned into an energy dependence by Fourier transforming the time series

$$\widetilde{\psi}_i(\mathbf{r}_S, E) = \frac{1}{\sqrt{2\pi}} \int \mathrm{e}^{-iEt} \psi_i(\mathbf{r}_S, t) \mathrm{d}t, \tag{76}$$

and the photoelectron energy distribution is postulated to be proportional to a sum over the orbitals in the following fashion:

$$P_{\mathbf{r}_S}(E) \propto \frac{1}{\sqrt{E}} \sum_{i=1}^{N} |\widetilde{\psi}_i(\mathbf{r}_S, E)|^2. \tag{77}$$

Because photoelectrons are in general emitted with different probabilities at different angles, a more accurate definition of the total probability is to sample the boundary densely with points $\mathbf{r}_S$ so that (77) becomes an integral over a surface S enclosing the system

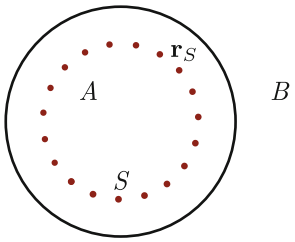

Fig. 12 Electron photoemission with the sampling method. The energy-resolved photoelectron probability is calculated by recording the time evolution of the wavefunction at the *points marked in red*

$$P(E) \propto \int_S P_{\mathbf{r}_S}(E) \mathrm{d}\mathbf{r}_S. \tag{78}$$

In practical calculations, the integral over the S is of course still discretized, and open boundary conditions, often in the form of absorbing boundaries, may be employed. The choice of the absorber must be such that it efficiently removes reflected wave packets in the energy range where photoelectrons are simulated.

In the original paper, (78) was introduced without the energy density factor $1/\sqrt{E}$ and the surface integral [95]. The results where thus, in general, strongly dependent on the choice of the sample point $\mathbf{r}_s$ and applicable only in the situations where the electrons are emitted as s-waves, hence not presenting any angular fluctuations. Even taking into account the integral over S, the method is not free from problems. It requires S to be placed at a distance from the parent system such that two conditions are fulfilled: (i) the electronic wave packets can be considered to be composed of outgoing waves only, and (ii) photoelectrons must hit the surface at a time for which the external field is turned off. It was later realized that a time- and energy-dependent phase $\mathrm{e}^{i\Phi(E,t)}$ must be included in the integral (76) to account for the wrong kinetic energy reference when the external field is still active [96].

Although this method is straightforward and easy to implement in existing TDDFT codes, the above drawbacks render it of limited use in many interesting physical situations, especially when strong laser fields are employed.

6.2 *Surface Flux Approach*

This method is based on the idea that differential photoemission probabilities (74) can be calculated by recording the electron flux through a surface. It was originally introduced by Scrinzi and co-workers in Caillat et al. [97] in the context of multi-configuration Hartree–Fock and then further developed in Scrinzi [98] and Tao and Scrinzi [99] for one- and two-electron problems. Although no applications in the context of TDDFT have been attempted so far, it presents an interesting approach for the calculation of photoelectron differential probabilities in bounded volumes.

Let us consider the case of a one-electron system governed by a Hamiltonian $\hat{H}(t)$ (71) such that at large distances it matches an exactly solvable one $\hat{H}_{\mathrm{v}}(t)$,

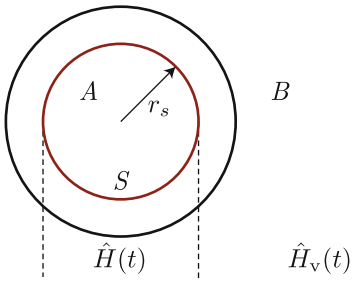

Fig. 13 The setup for the calculation of electron photoemission with the surface flux method. The emission probability is calculated by recording the flux through the closed surface *S marked in red*

$$\hat{H}(t) = \hat{H}_{\mathrm{v}}(t) \quad \text{for } |\mathbf{r}| \geq r_s \text{ and all } t, \tag{79}$$

as shown in Fig. 13. We are assuming here for simplicity that the surface S separating the Hamiltonians is spherical, but what follows can be easily extended to a generic surface. If we consider the case of a short range external potential $\nu_{\mathrm{ext}}(\mathbf{r}) = 0$ for $|\mathbf{r}| > r_s$, $\hat{H}_{\mathrm{v}}$ is the Volkov Hamiltonian, i.e., the Hamiltonian governing the motion of free electrons in an external field:

$$\hat{H}_{\mathrm{v}}(t) = \frac{1}{2}\left[-i\nabla - \frac{\boldsymbol{\mathcal{A}}(t)}{c}\right]^2. \tag{80}$$

Provided the external field has no spatial dependence, i.e., $\boldsymbol{\mathcal{A}}(t)$ is constant in space, the associated TDSE can be solved exactly. The solutions can then be expressed as plane waves with an additional time and momentum-dependent phase:

$$\phi_{\mathbf{k}}(\mathbf{r}, t) = \frac{1}{(2\pi)^{\frac{3}{2}}} e^{i\mathbf{k}\cdot\mathbf{r}} e^{-i\Phi(\mathbf{k},t)}, \quad \Phi(\mathbf{k}, t) = \frac{1}{2}\int_{-\infty}^{t} \left[\mathbf{k} - \frac{\boldsymbol{\mathcal{A}}(t)}{c}\right]^2 \mathrm{d}t'. \tag{81}$$

Let us imagine the situation where a laser pulse ionizes our system. In the long time limit $t > T$, some time after the field as been turned off, $\boldsymbol{\mathcal{A}}(t > T) = 0$, the electronic configuration is described by a scattering wavefunction which can be partitioned into bound and scattering components,

$$\Psi(\mathbf{r}, t) = \Psi_A(\mathbf{r}, t) + \Psi_B(\mathbf{r}, t), \tag{82}$$

which are approximately localized in the bound and unbound regions A and B of Fig. 8. The quality of this approximation is ultimately connected to r_s and T, and the time that it takes the slowest components of the scattering wave packet $\Psi_B(\mathbf{r},t)$ to cross S.

In order to calculate the emission amplitude, we just need to evaluate the projection of $\Psi(\mathbf{r},t)$ over the asymptotic wavefunctions $\phi_{\mathbf{k}}(\mathbf{r})$ as in (75). The information about the scattering process is contained only in $\Psi_B(\mathbf{r},t)$. Because $\Psi_B(\mathbf{r},t)$ is exponentially vanishing in A for $t \geq T$, we can write the emission amplitude as

$$S(\mathbf{k},T) = \langle \phi_{\mathbf{k}}(T)|\theta(\mathbf{r},r_s)|\Psi(T)\rangle = \big\langle \phi_{\mathbf{k}}(T)\big|\Psi_B(T)\big\rangle, \tag{83}$$

with $\theta(\mathbf{r},r_s)$ being a step function with support in B defined as

$$\theta(\mathbf{r},r_s) = \begin{cases} 0 & \text{for } |\mathbf{r}| < r_s \\ 1 & \text{for } |\mathbf{r}| \geq r_s \end{cases}. \tag{84}$$

Equation (83) can be written as a time integral of the derivative of $S(\mathbf{k},t)$. Combined with the Ehrenfest theorem and the fact that both states in (83) evolve with the same Hamiltonian $\hat{H}_{\mathrm{v}}$ within the support of $\theta(\mathbf{r},r_s)$ we obtain

$$S(\mathbf{k},T) = i\int_0^T \big\langle \phi_{\mathbf{k}}(t)\big|\big[\hat{H}_{\mathrm{v}},\theta(\mathbf{r},r_s)\big]\big|\Psi(t)\big\rangle \mathrm{d}t. \tag{85}$$

The dependence on T of the emission amplitude $S(\mathbf{k}, T)$ becomes negligible for large values of T. The momentum-resolved probability is then defined by taking the square modulus of the emission amplitude $P(\mathbf{k}) = |S(\mathbf{k}, T)|^2$ and dropping the dependence on T.

Equation (85) can be interpreted as the time integral of a surface flux, hence the name of the method. This interpretation can be established by observing that the commutator in (85) is non-zero only for $|\mathbf{r}| = r_s$, and that the expectation value reduces to an integral over S. We can also proceed one step further and explicitly write the emission amplitude as a flux integral

$$S(\mathbf{k},T) = \int_0^T \int_S \mathbf{J}_{\mathbf{k}}(t)\cdot \mathrm{d}\mathbf{r}_s \mathrm{d}t \tag{86}$$

of the momentum-resolved current density

$$\mathbf{J}_{\mathbf{k}}(t) = \frac{1}{2}\left[\Psi(t) i\nabla\phi^*_{\mathbf{k}}(t) - \phi^*_{\mathbf{k}}(t) i\nabla\Psi(t) - 2\frac{\boldsymbol{\mathcal{A}}(t)}{c}\phi^*_{\mathbf{k}}(t)\Psi(t)\right]. \tag{87}$$

In practical calculations the time propagation of $\Psi(t)$ can be spatially truncated, imposing open boundary conditions in the region outside S. The evaluation of $P(\mathbf{k})$ can then be safely performed in a bounded volume.

In order to obtain (85) we only need to find a Hamiltonian $\hat{H}_{\mathrm{v}}$ that satisfies the asymptotic condition (79). The method can, in principle, be extended to handle the long-range Coulomb potential just by modifying (80) to match the Coulomb tails. In this case, however, the calculation of $\phi_{\mathbf{k}}(\mathbf{r},t)$ is complicated by the absence of an exact solution for time-dependent $\boldsymbol{\mathcal{A}}(t)$ and the Coulomb–Volkov solutions provide a poor approximation [99]. In practical situations, the use of free Volkov wavefunctions (81) as asymptotic solution combined with a convergence on the surface radius r_s is nevertheless enough to provide high-quality results.

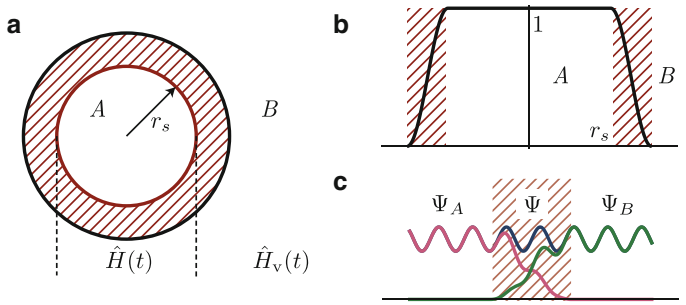

Fig. 14 The main traits of the mask method. In this method, photoelectrons are time propagated with a mixed real and momentum-space representation. A *red striped area* identifies the region where the matching between the two representations is performed. (**a**) Spatial and Hamiltonian partitioning. (**b**) The mask function. (**c**) A wavefunction Ψ is split into two parts, Ψ_A and Ψ_B, using the mask function

6.3 Mask Method

This *mask method* is based on the idea that the photoelectron emission probability can be calculated by explicitly propagating the ionized electron wave packets as a superposition of plane waves. The problem of matching inner and outer solutions is solved here with the aid of a mask function [90]. This approach as been successfully employed within TDDFT in situations involving atoms and molecules under the influence of a variety of external fields ranging from strong and weak laser fields [90] to pump and probe configurations [100, 101].

We begin here by introducing the equations governing time propagation for the single-electron case and then turn to the many-electron one. Let us consider the case where the Hamiltonian $\hat{H}(t)$ is of short range and satisfies the asymptotic condition (79), i.e., it coincides with $\hat{H}_v(t)$ for $|\mathbf{r}| \geq r_s$ as illustrated in Fig. 14a.

As discussed in the previous section, in the long-time limit of an ionization process, we can assume the electronic wavefunction splits into two spatially separated parts, namely the bound and the scattering parts (82). A practical way to implement this splitting for a generic time t is to use a mask function $M(\mathbf{r})$ similar to what was discussed in Sect. 5.5:

$$\Psi(\mathbf{r},t) = M(\mathbf{r})\Psi(\mathbf{r},t) + [1 - M(\mathbf{r})]\Psi(\mathbf{r},t) = \Psi_A(\mathbf{r},t) + \Psi_B(\mathbf{r},t). \qquad (88)$$

We consider here the case where $M(\mathbf{r})$ is a continuous function equal to 1 in an inner part of A, where $|\mathbf{r}| \leq r_s$, equal to 0 in B, and smoothly decays over the intermediate region as shown in Fig. 14b. The splitting defined with this procedure is smooth and the wavefunctions $\Psi_A(\mathbf{r},t)$ and $\Psi_B(\mathbf{r},t)$ are not sharply separated but are allowed to overlap in the region where the mask decays to zero, as illustrated in Fig. 14c. The mask function $M(\mathbf{r})$ is such that this overlap region is entirely contained in A.

The solution of the TDSE associated with the full Hamiltonian $\hat{H}(t)$ in the whole space $A \cup B$ can be formally written as a set of coupled equations:

$$\begin{cases} |\Psi_A(t')\rangle = \hat{M}\,\hat{U}\,(t',t)[|\Psi_A(t)\rangle + |\Psi_B(t)\rangle] \\ |\Psi_B(t')\rangle = \left[1-\hat{M}\right]\hat{U}\,(t',t)[|\Psi_A(t)\rangle + |\Psi_B(t)\rangle] \end{cases}, \tag{89}$$

using the time evolution operator

$$\hat{U}\,(t',t) = \exp\left\{-i\int_t^{t'} \hat{H}\,(\tau)\mathrm{d}\tau\right\}, \tag{90}$$

and imposing the boundary condition $|\Psi_B(t=0)\rangle = 0$. Here the mask operator is given by $\langle \mathbf{r}|\mathrm{P}\hat{M}\,|\mathbf{r}'\rangle = M(\mathbf{r})\delta(\mathbf{r}-\mathbf{r}')$.

Owing to the asymptotic condition (79) on the Hamiltonian, $|\Psi_B(t)\rangle$ evolves under the action of $\hat{H}_\mathrm{v}$ defined in (80). In what follows we indicate with $U_\mathrm{v}(t',t)$ the evolution operator associated with $\hat{H}_\mathrm{v}$. Because $\hat{H}_\mathrm{v}$ is diagonal in momentum, the action of $U_\mathrm{v}(t',t)$ is easily described in this space. It is thus convenient to expand the equations for $|\Psi_B(t)\rangle$ using plane waves: $\langle \mathbf{r}|\mathbf{k}\rangle = (2\pi)^{-3/2}\exp\{i\mathbf{k}\cdot\mathbf{r}\}$. On the other hand, owing to the presence in $\hat{H}(t)$ of $V(\mathbf{r})$, which has an explicit dependence on $\mathbf{r}$, the equations for $|\Psi_A(t)\rangle$ are better solved in real space. The use of a mixed real and momentum space representation seems the more natural one for the problem.

Using a mixed representation we can integrate (89) by recursively applying the discrete time evolution operator $\hat{U}(\Delta t) \equiv \hat{U}(t+\Delta t,t)$ as

$$\begin{cases} \langle \mathbf{r}|\Psi_A(t+\Delta t)\rangle = \langle \mathbf{r}|\hat{M}\,\hat{U}\,(\Delta t)|\Psi_A(t)\rangle + \langle \mathbf{r}|\hat{M}\,\hat{U}_\mathrm{v}(\Delta t)|\Psi_B(t)\rangle \\ \langle \mathbf{k}|\Psi_B(t+\Delta t)\rangle = \langle \mathbf{k}|\left[1-\hat{M}\right]\hat{U}\,(\Delta t)|\Psi_A(t)\rangle + \langle \mathbf{k}|\left[1-\hat{M}\right]\hat{U}_\mathrm{v}(\Delta t)|\Psi_B(t)\rangle \end{cases}, \tag{91}$$

with initial condition $\langle \mathbf{k}|\Psi_B(t=0)\rangle = 0$. These equations can be written in a closed form for $\langle \mathbf{r}|\Psi_A(t)\rangle$ and $\langle \mathbf{k}|\Psi_B(t)\rangle$ by including the additional set

$$\begin{cases} \langle \mathbf{r}|\hat{M}\,\hat{U}\,(\Delta t)|\Psi_A(t)\rangle = M(\mathbf{r})\langle \mathbf{r}|\hat{U}\,(\Delta t)|\Psi_A(t)\rangle \\ \langle \mathbf{r}|\hat{M}\,\hat{U}_\mathrm{v}(\Delta t)|\Psi_B(t)\rangle = M(\mathbf{r})\displaystyle\int \langle \mathbf{r}|\mathbf{k}\rangle\langle \mathbf{k}|\hat{U}_\mathrm{v}(\Delta t)|\Psi_B(t)\rangle \mathrm{d}\mathbf{k} \\ \langle \mathbf{k}|\left[1-\hat{M}\right]\hat{U}\,(\Delta t)|\Psi_A(t)\rangle = \displaystyle\int \langle \mathbf{k}|\mathbf{r}\rangle[1-M(\mathbf{r})]\langle \mathbf{r}|\hat{U}\,(\Delta t)|\Psi_A(t)\rangle \mathrm{d}\mathbf{r} \\ \langle \mathbf{k}|\left[1-\hat{M}\right]\hat{U}_\mathrm{v}(\Delta t)|\Psi_B(t)\rangle = \langle \mathbf{k}|\hat{U}_\mathrm{v}(\Delta t)|\Psi_B(t)\rangle - \displaystyle\int \langle \mathbf{k}|\mathbf{r}\rangle\langle \mathbf{r}|\hat{M}\,\hat{U}_\mathrm{v}(\Delta t)|\Psi_B(t)\rangle \mathrm{d}\mathbf{r} \end{cases}. \tag{92}$$

The equations in (92) have an intuitive interpretation in terms of electron flow. The first and second equations account, respectively, for electrons leaving and returning to A. The third equation is responsible for introducing charge in B whereas the fourth is composed of a term of pure time evolution minus a term balancing the backward flow of the second equation. In the limit of infinitesimal steps $\Delta t = dt$, the complete set defined by (91) and (92) is equivalent to (89), and it fully accounts

for the description of outgoing and incoming particle flows. In this respect it directly relates to the exact boundary conditions of Sect. 5.1.

Once (91) and (92) are propagated up to a time T such that the external field has vanished and the bound and scattering components of $\Psi(t)$ are well separated, the momentum-resolved probability can be obtained just by taking the square modulus of the wavefunction in B: $P(\mathbf{k}) = |\langle \mathbf{k}|\Psi_B(T)\rangle|^2$. This definition is consistent with that of the surface flux method, noting that, at time T, Volkov and plane waves differ only by a phase $|\phi_{\mathbf{k}}(T)\rangle = |\mathbf{k}\rangle \exp\{i\Phi(\mathbf{k},T)\}$. Extending the mask method to the case of infinite-range potentials incurs the same approximation errors as in the flux method with Volkov states.

The extension of the method to the many-electron case, on the other hand, is less trivial. It can be derived from a phase-space standpoint given the interpretation of the Wigner transform of the one-body density matrix $\rho(\mathbf{r},\mathbf{r}',t)$,

$$W(\mathbf{R},\mathbf{k},t) = \int \frac{\mathrm{e}^{i\mathbf{k}\cdot\mathbf{s}}}{(2\pi)^{\frac{3}{2}}} \rho\left(\mathbf{R}+\frac{\mathbf{s}}{2},\mathbf{R}-\frac{\mathbf{s}}{2},t\right)\mathrm{d}\mathbf{s} \quad \text{with} \quad \begin{cases} \mathbf{R} = (\mathbf{r}+\mathbf{r}')/2 \\ \mathbf{s} = \mathbf{r}-\mathbf{r}' \end{cases}, \tag{93}$$

as a quasi-probability distribution. With this interpretation it is natural to define the photoemission probability as the integral over B of $W(\mathbf{R},\mathbf{k},t)$, i.e.,

$$P(\mathbf{k}) = \lim_{t\to\infty} \int_B W(\mathbf{R},\mathbf{k},t)\mathrm{d}\mathbf{R}. \tag{94}$$

The connection with TDDFT can be established using the Kohn–Sham one-body density matrix

$$\rho_{\mathrm{KS}}(\mathbf{r},\mathbf{r}',t) = 2\sum_{i=1}^{N/2} \psi_i^*(\mathbf{r},t)\psi_i(\mathbf{r}',t) \tag{95}$$

in (93) to calculate the Wigner distribution. For simplicity we assume here a closed-shell system where each orbital $\psi_i(\mathbf{r},t)$ is doubly occupied. There is no fundamental restriction in extending to the more general case where spin polarization is taken into account.

We now assume that it is possible to establish an approximate asymptotic connection, similar to (79), between the Kohn–Sham Hamiltonian $\hat{H}_{\mathrm{KS}}(t)$ and $\hat{H}_{\mathrm{v}}(t)$ after a certain radius $|\mathbf{r}| > r_s$ (see De Giovannini et al. [90]). Under this assumption we can partition each orbital according to (88) and use (91) and (92) to propagate them in time. By plugging the Wigner distribution obtained from $\rho_{\mathrm{KS}}(\mathbf{r},\mathbf{r}',t)$ into (94) we then obtain that the momentum-resolved probability distribution can be expressed as an sum of orbital densities

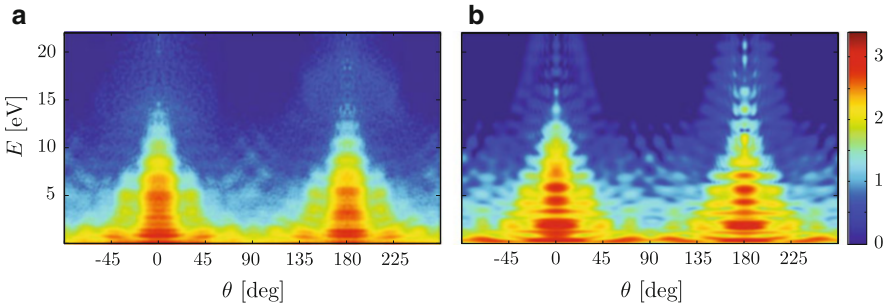

Fig. 15 Ionization of randomly oriented N_2 molecules by a strong infrared laser field. Angle and energy-resolved photoelectron probability $P(E,\theta)$ (log scale) obtained from the experiment [102] (**a**) and with the theory (**b**) using the mask method of (91) and (92). The laser is a six-cycle pulse with wavelength $\lambda = 750$ nm and intensity $I = 4.3 \times 10^{13}$ W/cm^2. Adapted from De Giovannini et al. [90]

$$P(\mathbf{k}) = 2\sum_{i=1}^{N/2} \left| \langle \mathbf{k} | \psi_{i,B}(T) \rangle \right|^2. \tag{96}$$

The quality of this approximation is now limited by the error committed by truncating the exchange and correlation potential contained in $\hat{H}_{\mathrm{KS}}(t)$ for $\mathbf{r} \geq r_s$. In atoms and molecules this adds to the error from truncating the tails of the Coulomb potential and strongly depends on the dynamics induced by the external field. It should be noted that for independent electrons in short-range potentials the method is exact. The validity of this approximation in more general situations may be assessed on the basis of the success in reproducing experiments. The example constituted by the strong field ionization of N_2 in Fig. 15 offers a good argument in favor of its success.

In numerical implementations the evaluations of the integrals in (92) must undergo some level of discretization. In spite of the fact that the integrands can be safely assumed to be well localized both in real and momentum space, the discretization process turns out to be a limiting factor. In fact, substituting Fourier integrals by Fourier series introduces unwanted periodic boundaries conditions that reintroduce ionized wave packets into the simulation box. This results in a limit for the maximum time a simulation can be carried on as the time needed for the fastest wave packet to reenter A. For a more detailed discussion see the appendix of De Giovannini et al. [90].

A more stable scheme can be obtained by simplifying (92) under the assumption that the electron flow is only outward from A. In this case we can set to zero the term responsible for the introduction of charge from B, and obtain a modified set of equations:

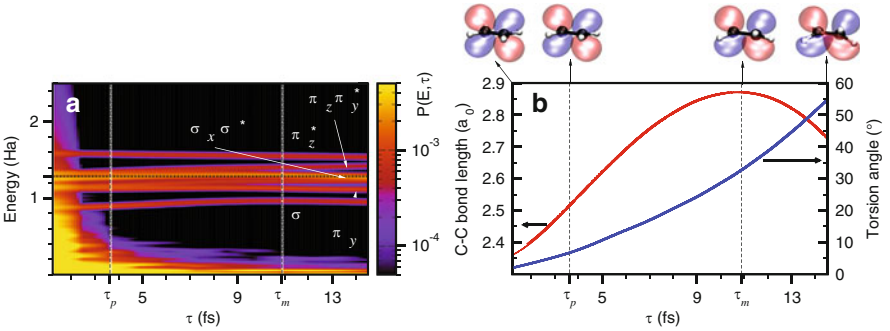

Fig. 16 Relaxation of a $\pi_z \rightarrow \pi_z^*$ excitation in ethylene observed with photoelectrons calculated with (91) and (97). (**a**) Time-resolved photoelectron spectrum $P(E, \tau)$ as a function of electron energy E and time delay τ from the initial excitation measured with an XUV probe pulse of energy $\omega = 1.8$ a.u., with a 40-cycle trapezoidal shape (8-cycle ramp), and an intensity of $I = 1.02 \times 10^{11}$ W/cm^2. (**b**) Carbon–carbon bond length in *red* and torsion angle in *blue* as a function of the time delay τ. Nuclear motion is modeled classically with an initial temperature of 300 K. Adapted from Crawford-Uranga et al. [100]

$$\begin{cases} \langle \mathbf{r}|\hat{M}\,\hat{U}\,(\Delta t)|\Psi_A(t)\rangle = M(\mathbf{r})\langle \mathbf{r}|\hat{U}\,(\Delta t)|\Psi_A(t)\rangle \\ \langle \mathbf{r}|\hat{M}\,\hat{U}_{\mathrm{v}}(\Delta t)|\Psi_B(t)\rangle = 0 \\ \langle \mathbf{k}|\left[1-\hat{M}\right]\hat{U}\,(\Delta t)|\Psi_A(t)\rangle = \int \langle \mathbf{k}|\mathbf{r}\rangle[1-M(\mathbf{r})]\langle \mathbf{r}|\hat{U}\,(\Delta t)|\Psi_A(t)\rangle \mathrm{d}\mathbf{r} \\ \langle \mathbf{k}|\left[1-\hat{M}\right]\hat{U}_{\mathrm{v}}(\Delta t)|\Psi_B(t)\rangle = \langle \mathbf{k}|\hat{U}_{\mathrm{v}}(\Delta t)|\Psi_B(t)\rangle \end{cases} . \tag{97}$$

Together with (91), it defines a modified scheme completely equivalent to the previous one in the limit where r_s is big enough to justify the outgoing flow condition. The distance at which this condition is satisfied ultimately depends on the electron dynamics induced by the external fields.

In (97) the first two equations, which govern the evolution of the real-space components of the wavefunction in A, are no longer connected with the momentum-space ones, and the propagation is thus equivalent to a time propagation with a mask function absorber similar to that in (66). The new more stable scheme thus comes at the price of introducing spurious reflections. Such reflections can, in principle, be reduced by using the most appropriate MFA or a CAP connected via equation (67). In the energy range where the MFA is absorbing, it is possible to carry out stable simulations for long times. As an example, in Fig. 16 we show the time-resolved photoelectron spectrum for an ethylene molecule where the ionic degrees of freedom are included at a classical level [100].

7 Summary

We have discussed a selection of methods which in different ways allow the calculation of properties of open quantum systems, with the objective of describing electron emission processes.

In scattering experiments and spectroscopy, the concept of resonances is of particular importance, and we have taken care to describe in detail the complex scaling method which, by a transformation of the real-space coordinates, causes the exponentially divergent resonant states to localize and become representable as square integrable states which emerge as eigenstates of the transformed, non-Hermitian Hamiltonian. This, to a large extent, makes them accessible using standard bound-state methods. The extension of ordinary ground-state DFT with complex scaling allows for a computationally tractable means of extracting resonant states and properties such as energy and lifetimes in many-body systems.

Although resonances can be captured from static calculations reminiscent of ground-state DFT, truly dynamic processes require explicit time propagation approaches. We have subsequently examined several methods used to describe dynamics leading to electron emission. We have studied these methods from the perspective of a complex system A which is in contact with a different system B that acts as a reservoir. Representing the wavefunction in B by means of Green functions provides a flexible way of accessing the full open-boundary problem, allowing transfer of particles into and out of a system. Using Green function embedding, one can calculate the wavefunctions in A that automatically satisfy the boundary conditions emulating their contact with B. However such embedding techniques suffer the disadvantage of being computationally demanding when employed to solve fully three-dimensional problems with first-principles methods.

Absorbing boundaries provide more computationally practical ways of accessing ionization processes in which charge leaves the system. We have considered absorbing boundaries and mask functions which are simple methods to absorb outgoing waves in time-dependent simulations. The boundary absorbers are meant to absorb waves that leave the system, so that an outgoing wave disappears rather than reflects on the simulation box. The complex scaling method provides a particularly elegant way to absorb outgoing waves, allowing one, in principle, to impose perfectly absorbing boundaries.

Having discussed the problem of describing total ionization with the appropriate choice of boundary conditions, we turned to the problem of describing electron photoemission probabilities with TDDFT. We examined three approaches suitable for the task. The sampling point method, where the energy-resolved probability is calculated by Fourier transforming the time evolution of each Khon–Sham orbital in the energy domain; the surface flux method, where the photoelectron probability is generated by recording the electron flux through a closed surface surrounding the system; and finally we discussed the mask method where, by means of a mask function, it is possible to generate a split real/momentum-space propagation scheme where electrons, moving from a bounded volume into the empty space, seamlessly

change from real space to momentum space representation. This scheme allows for the description of a wide range of processes and time resolved pump–probe spectroscopies.

Acknowledgments We acknowledge financial support from the European Research Council Advanced Grant DYNamo (ERC-2010-AdG-267374), Ministerio de Economía y Competitividad or MINECO, Spanish Grant (FIS2013-46159-C3-1-P), Grupos Consolidados UPV/EHU del Gobierno Vasco (IT578-13), European Commission FP7 project CRONOS (Grant number 280879-2), COST Actions CM1204 (XLIC), and MP1306 (EUSpec).

References

1. Hohenberg P, Kohn W (1964) Inhomogeneous electron gas. Phys Rev 136:B864–B871. doi:10.1103/PhysRev.136.B864, http://link.aps.org/doi/10.1103/PhysRev.136.B864
2. Runge E, Gross EKU (1984) Density-functional theory for time-dependent systems. Phys Rev Lett 52(12):997–1000
3. Kohn W, Sham LJ (1965) Self-consistent equations including exchange and correlation effects. Phys Rev 140:A1133–A1138. doi:10.1103/PhysRev.140.A1133, http://link.aps.org/doi/10.1103/PhysRev.140.A1133
4. Burke K, Car R, Gebauer R (2005) Density functional theory of the electrical conductivity of molecular devices. Phys Rev Lett 94(14):146803
5. Tempel DG, Aspuru-Guzik A (2011) Relaxation and dephasing in open quantum systems time-dependent density functional theory: properties of exact functionals from an exactly-solvable model system. Chem Phys 391(1):130–142
6. Tempel DG, Watson MA, Olivares-Amaya R, Aspuru-Guzik A (2011) Time-dependent density functional theory of open quantum systems in the linear-response regime. J Chem Phys 134(7):074116
7. Yuen-Zhou J, Rodríguez-Rosario C, Aspuru-Guzik A (2009) Time-dependent current-density functional theory for generalized open quantum systems. Phys Chem Chem Phys 11(22):4509–4522
8. Yuen-Zhou J, Tempel DG, Rodríguez-Rosario CA, Aspuru-Guzik A (2010) Time-dependent density functional theory for open quantum systems with unitary propagation. Phys Rev Lett 104(4):043001
9. Marques MAL, Maitra NT, Nogueira F, Gross EKU, Rubio A (2011) Fundamentals of time-dependent density functional theory. Springer, Berlin
10. Fano U (1961) Effects of configuration interaction on intensities and phase shifts. Phys Rev 124(6):1866–1878
11. Brandbyge M, Mozos JL, Ordejón P, Taylor J, Stokbro K (2002) Density-functional method for nonequilibrium electron transport. Phys Rev B 65:165401. doi:10.1103/PhysRevB.65.165401
12. Chen J, Thygesen KS, Jacobsen KW (2012) Ab initio. Phys Rev B 85:155140. doi:10.1103/PhysRevB.85.155140, http://link.aps.org/doi/10.1103/PhysRevB.85.155140
13. Larsen AH, Vanin M, Mortensen JJ, Thygesen KS, Jacobsen KW (2009) Localized atomic basis set in the projector augmented wave method. Phys Rev B 80:195112. doi:10.1103/PhysRevB.80.195112, http://link.aps.org/doi/10.1103/PhysRevB.80.195112
14. Soler JM, Artacho E, Gale JD, García A, Junquera J, Ordejón P, Sánchez-Portal D (2002) The SIESTA method for ab initio order-N materials simulation. J Phys Condens Matter 14:2745–2779. doi:10.1088/0953-8984/14/11/302, http://iopscience.iop.org/0953-8984/14/11/302

15. Newns DM (1969) Self-consistent model of hydrogen chemisorption. Phys Rev 178: 1123–1135. doi:10.1103/PhysRev.178.1123, http://link.aps.org/doi/10.1103/PhysRev.178.1123
16. Gellene GI (1995) Resonant states of a one-dimensional piecewise constant potential. J Chem Educ 72(11):1015. doi:10.1021/ed072p1015, http://dx.doi.org/10.1021/ed072p1015
17. Siegert AJF (1939) On the derivation of the dispersion formula for nuclear reactions. Phys Rev 56:750–752. doi:10.1103/PhysRev.56.750, http://link.aps.org/doi/10.1103/PhysRev.56.750
18. Hatano N, Sasada K, Nakamura H, Petrosky T (2008) Some properties of the resonant state in quantum mechanics and its computation. Prog Theor Phys 119(2):187–222. doi:10.1143/PTP.119.187, http://ptp.oxfordjournals.org/content/119/2/187.abstract
19. Aguilar J, Combes J (1971) A class of analytic perturbations for one-body Schrödinger Hamiltonians. Commun Math Phys 22:269–279. doi:10.1007/BF01877510, http://dx.doi.org/10.1007/BF01877510
20. Balslev E, Combes JM (1971) Spectral properties of many-body Schrödinger operators with dilatation-analytic interactions. Commun Math Phys 22(4):280–294
21. Simon B (1973) Resonances in n-body quantum systems with dilatation analytic potentials and the foundations of time-dependent perturbation theory. Ann Math 97:247–274
22. Simon B (1979) The definition of molecular resonance curves by the method of exterior complex scaling. Phys Lett A 71(2):211–214
23. Ho Y (1983) The method of complex coordinate rotation and its applications to atomic collision processes. Phys Rep 99(1):1–68. doi:10.1016/0370-1573(83)90112-6, http://www.sciencedirect.com/science/article/pii/0370157383901126
24. McCurdy CW, Baertschy M, Rescigno TN (2004) Solving the three-body Coulomb breakup problem using exterior complex scaling. J Phys B At Mol Opt 37(17):R137, http://stacks.iop.org/0953-4075/37/i=17/a=R01
25. Moiseyev N (1998) Quantum theory of resonances: calculating energies, widths and cross-sections by complex scaling. Phys Rep 302(5–6):212–293. doi:10.1016/S0370-1573(98)00002-7, http://www.sciencedirect.com/science/article/pii/S0370157398000027
26. Reinhardt WP (1982) Complex coordinates in the theory of atomic and molecular structure and dynamics. Annu Rev Phys Chem 33(1):223–255. doi:10.1146/annurev.pc.33.100182.001255, http://www.annualreviews.org/doi/abs/10.1146/annurev.pc.33.100182.001255
27. Simon B (1978) Resonances and complex scaling: a rigorous overview. Int J Quantum Chem 14(4):529–542. doi:10.1002/qua.560140415, http://dx.doi.org/10.1002/qua.560140415
28. Cerjan C, Hedges R, Holt C, Reinhardt WP, Scheibner K, Wendoloski JJ (1978) Complex coordinates and the Stark effect. Int J Quantum Chem 14(4):393–418. doi:10.1002/qua.560140408, http://dx.doi.org/10.1002/qua.560140408
29. Herbst IW (1979) Dilation analyticity in constant electric field. Commun Math Phys 64(3): 279–298. doi:10.1007/BF01221735
30. Herbst IW, Simon B (1978) Stark effect revisited. Phys Rev Lett 41:67–69. doi:10.1103/PhysRevLett.41.67, http://link.aps.org/doi/10.1103/PhysRevLett.41.67
31. Scrinzi A, Piraux B (1998) Two-electron atoms in short intense laser pulses. Phys Rev A 58: 1310–1321. doi:10.1103/PhysRevA.58.1310, http://link.aps.org/doi/10.1103/PhysRevA.58.1310
32. Junker BR (1983) Complex virial theorem and complex scaling. Phys Rev A 27:2785–2789. doi:10.1103/PhysRevA.27.2785, http://link.aps.org/doi/10.1103/PhysRevA.27.2785
33. Moiseyev N, Friedland S, Certain PR (1981) Cusps, θ trajectories, and the complex virial theorem. J Chem Phys 74(8):4739–4740. doi:10.1063/1.441624, http://scitation.aip.org/content/aip/journal/jcp/74/8/10.1063/1.441624
34. McCurdy CW (1980) Complex-coordinate calculation of matrix elements of the resolvent of the Born–Oppenheimer Hamiltonian. Phys Rev A 21:464–470. doi:10.1103/PhysRevA.21.464, http://link.aps.org/doi/10.1103/PhysRevA.21.464
35. McCurdy CW, Rescigno TN (1978) Extension of the method of complex basis functions to molecular resonances. Phys Rev Lett 41:1364–1368. doi:10.1103/PhysRevLett.41.1364, http://link.aps.org/doi/10.1103/PhysRevLett.41.1364

36. Moiseyev N, Corcoran C (1979) Autoionizing states of H_2 and H_2^- using the complex-scaling method. Phys Rev A 20:814–817. doi:10.1103/PhysRevA.20.814, http://link.aps.org/doi/10.1103/PhysRevA.20.814
37. Morgan JD, Simon B (1981) The calculation of molecular resonances by complex scaling. J Phys B At Mol Opt 14(5):L167
38. Scrinzi A (2010) Infinite-range exterior complex scaling as a perfect absorber in time-dependent problems. Phys Rev A 81(5):053845
39. Moiseyev N (1999) Derivations of universal exact complex absorption potentials by the generalized complex coordinate method. J Phys B At Mol Opt 31(7):1431–1441
40. Krylstedt P, Carlsund C, Elander N (1989) On the calculation of electron–atom collision properties using exterior complex dilatated *s*-matrix expansions. J Phys B At Mol Opt 22(7): 1051, http://stacks.iop.org/0953-4075/22/i = 7/a = 014
41. Rescigno TN, Baertschy M, Byrum D, McCurdy CW (1997) Making complex scaling work for long-range potentials. Phys Rev A 55:4253–4262. doi:10.1103/PhysRevA.55.4253, http://link.aps.org/doi/10.1103/PhysRevA.55.4253
42. Scrinzi A, Elander N (1993) A finite element implementation of exterior complex scaling for the accurate determination of resonance energies. J Chem Phys 98(5):3866–3875. doi:10.1063/1.464014, http://scitation.aip.org/content/aip/journal/jcp/98/5/10.1063/1.464014
43. Simons J (1980) The complex coordinate rotation method and exterior scaling: a simple example. Int J Quantum Chem 18(S14):113–121. doi:10.1002/qua.560180814, http://dx.doi.org/10.1002/qua.560180814
44. Kar S, Ho YK (2009) Isotope shift for the $^1D^e$ autodetaching resonance in H^- and D^-. J Phys B At Mol Opt 42(5):055001, http://stacks.iop.org/0953-4075/42/i = 5/a = 055001
45. Scrinzi A, Geissler M, Brabec T (1999) Ionization above the Coulomb barrier. Phys Rev Lett 83:706–709. doi:10.1103/PhysRevLett.83.706, http://link.aps.org/doi/10.1103/PhysRevLett.83.706
46. McCurdy CW, Rescigno TN, Davidson ER, Lauderdale JG (1980) Applicability of self-consistent field techniques based on the complex coordinate method to metastable electronic states. J Chem Phys 73(7):3268–3273. doi:10.1063/1.440522, http://scitation.aip.org/content/aip/journal/jcp/73/7/10.1063/1.440522
47. Samanta K, Yeager DL (2008) Investigation of ^2P Be^- shape resonances using a quadratically convergent complex multiconfigurational self-consistent field method. J Phys Chem B 112(50):16214–16219. doi:10.1021/jp806998n, http://dx.doi.org/10.1021/jp806998n
48. Zdánská PR, Moiseyev N (2005) Hartree–Fock orbitals for complex-scaled configuration interaction calculation of highly excited Feshbach resonances. J Chem Phys 123(19):194105. doi:10.1063/1.2110169, http://scitation.aip.org/content/aip/journal/jcp/123/19/10.1063/1.2110169
49. Larsen AH, Whitenack DL, De Giovannini U, Wasserman A, Rubio A (2013) Stark ionization of atoms and molecules within density functional resonance theory. J Phys Chem Lett 4:2734–2738
50. Whitenack DL, Wasserman A (2011) Density functional resonance theory of unbound electronic systems. Phys Rev Lett 107(16):163002
51. Wasserman A, Moiseyev N (2007) Hohenberg-Kohn theorem for the lowest-energy resonance of unbound systems. Phys Rev Lett 98:093003. doi:10.1103/PhysRevLett.98.093003, http://link.aps.org/doi/10.1103/PhysRevLett.98.093003
52. Perdew JP, Wang Y (1992) Accurate and simple analytic representation of the electron-gas correlation energy. Phys Rev B 45:13244–13249. doi:10.1103/PhysRevB.45.13244, http://link.aps.org/doi/10.1103/PhysRevB.45.13244
53. Telnov DA, Sosnova KE, Rozenbaum E, Chu SI (2013) Exterior complex scaling method in time-dependent density-functional theory: multiphoton ionization and high-order-harmonic generation of Ar atoms. Phys Rev A 87(5):053406

54. van Leeuwen R, Baerends EJ (1994) Exchange–correlation potential with correct asymptotic behavior. Phys Rev A 49:2421–2431. doi:10.1103/PhysRevA.49.2421, http://link.aps.org/doi/10.1103/PhysRevA.49.2421
55. Ammosov MV, Delone NB, Krainov VP (1986) Tunnel ionization of complex atoms and atomic ions in a varying electromagnetic-field. Zh Éksp Teor Fiz 91:2008–2013
56. Parker SD, McCurdy C (1989) Propagation of wave packets using the complex basis function method. Chem Phys Lett 156(5):483–488. doi:10.1016/S0009-2614(89)87316-6, http://www.sciencedirect.com/science/article/pii/S0009261489873166
57. Bengtsson J, Lindroth E, Selstø S (2008) Solution of the time-dependent Schrödinger equation using uniform complex scaling. Phys Rev A 78:032502. doi:10.1103/PhysRevA.78.032502, http://link.aps.org/doi/10.1103/PhysRevA.78.032502
58. Bengtsson J, Lindroth E, Selstø S (2012) Wave functions associated with time-dependent, complex-scaled Hamiltonians evaluated on a complex time grid. Phys Rev A 85:013419. doi:10.1103/PhysRevA.85.013419, http://link.aps.org/doi/10.1103/PhysRevA.85.013419
59. Gilary I, Fleischer A, Moiseyev N (2005) Calculations of time-dependent observables in non-Hermitian quantum mechanics: the problem and a possible solution. Phys Rev A 72:012,117. doi:10.1103/PhysRevA.72.012117, http://link.aps.org/doi/10.1103/PhysRevA.72.012117
60. García-Moliner F, Flores F (2009) Introduction to the theory of solid surfaces. Cambridge University Press, Cambridge
61. Kudrnovský J, Drchal V, Turek I, Weinberger P (1994) Magnetic coupling of interfaces: a surface-Green's-function approach. Phys Rev B 50:16105–16108. doi:10.1103/PhysRevB.50.16105, http://link.aps.org/doi/10.1103/PhysRevB.50.16105
62. Boucke K, Schmitz H, Kull HJ (1997) Radiation conditions for the time-dependent Schrödinger equation: application to strong-field photoionization. Phys Rev A 56(1):763–771
63. Ermolaev A, Puzynin I, Selin A, Vinitsky S (1999) Integral boundary conditions for the time-dependent Schrödinger equation: atom in a laser field. Phys Rev A 60(6):4831–4845
64. Hellums J, Frensley W (1994) Non-Markovian open-system boundary conditions for the time-dependent Schrödinger equation. Phys Rev B 49(4):2904–2906
65. Kurth S, Stefanucci G, Almbladh CO, Rubio A, Gross EKU (2005) Time-dependent quantum transport: a practical scheme using density functional theory. Phys Rev B 72(3):035308
66. Inglesfield JE (2001) Embedding at surfaces. Comput Phys Commun 137(1):89–107
67. Inglesfield JE (2011) A time-dependent embedding calculation of surface electron emission. J Phys Condens Matter 23(30):305004
68. Antoine X, Arnold A, Besse C, Ehrhardt M, Schädle A (2008) A review of transparent and artificial boundary conditions techniques for linear and nonlinear Schrödinger equations. Commun Comput Phys 4:729–796
69. Inglesfield JE (1981) A method of embedding. J Phys C Solid State 14(26):3795–3806
70. Inglesfield J (2008) Time-dependent embedding. J Phys Condens Matter 20:095215
71. Ehrhardt M (1999) Discrete transparent boundary conditions for general Schrödinger-type equations. VLSI Des 9(4):325–338
72. Szmytkowski R, Bielski S (2004) Dirichlet-to-Neumann and Neumann-to-Dirichlet embedding methods for bound states of the Schrödinger equation. Phys Rev A 70(4):042103
73. Frensley W (1990) Boundary conditions for open quantum systems driven far from equilibrium. Rev Mod Phys 62(3):745–791
74. De Giovannini U, Larsen AH, Rubio A (2015) Modeling electron dynamics coupled to continuum states in finite volumes. Eur Phys J B 88(3):56. doi:10.1140/epjb/e2015-50808-0
75. Neuhauser D, Baer M (1989) The application of wave packets to reactive atom–diatom systems: a new approach. J Chem Phys 91(8):4651–4657
76. Neuhauser D, Baer M (1989) The time-dependent Schrödinger equation: application of absorbing boundary conditions. J Chem Phys 90(8):4351
77. Berenger JP (1994) A perfectly matched layer for the absorption of electromagnetic waves. J Comput Phys 114(2):185–200

78. Elenewski JE, Chen H (2014) Real-time transport in open quantum systems from PT-symmetric quantum mechanics. Phys Rev B 90(8):085104
79. Varga K, Pantelides S (2007) Quantum transport in molecules and nanotube devices. Phys Rev Lett 98(7):076804
80. Wibking BD, Varga K (2012) Quantum mechanics with complex injecting potentials. Phys Lett A 376(4):365–369
81. Muga J, Palao JP, Navarro B, Egusquiza IL (2004) Complex absorbing potentials. Phys Rep 395(6):357–426
82. Andrade X, Aspuru-Guzik A (2011) Prediction of the derivative discontinuity in density functional theory from an electrostatic description of the exchange and correlation potential. Phys Rev Lett 107(18):183002
83. Perdew JP, Burke K, Ernzerhof M (1996) Generalized gradient approximation made simple. Phys Rev Lett 77(18):3865–3868
84. Crawford-Uranga A, De Giovannini U, Räsänen E, Oliveira MJT, Mowbray DJ, Nikolopoulos GM, Karamatskos ET, Markellos D, Lambropoulos P, Kurth S, Rubio A (2014) Time-dependent density-functional theory of strong-field ionization of atoms by soft X-rays. Phys Rev A 90(3):033412
85. Krause J, Schafer K, Kulander K (1992) Calculation of photoemission from atoms subject to intense laser fields. Phys Rev A 45(7):4998–5010
86. Kulander K, Mies F, Schafer K (1996) Model for studies of laser-induced nonlinear processes in molecules. Phys Rev A 53(4):2562–2570
87. Lein M, Marangos J, Knight P (2002) Electron diffraction in above-threshold ionization of molecules. Phys Rev A 66(5):051404R
88. Chelkowski S, Foisy C, Bandrauk AD (1998) Electron–nuclear dynamics of multiphoton H_2^+ dissociative ionization in intense laser fields. Phys Rev A 57(2):1176–1185
89. Grobe R, Haan S, Eberly J (1999) A split-domain algorithm for time-dependent multi-electron wave functions. Comput Phys Commun 117(3):200–210
90. De Giovannini U, Varsano D, Marques MAL, Appel H, Gross EKU, Rubio A (2012) *Ab initio* angle- and energy-resolved photoelectron spectroscopy with time-dependent density-functional theory. Phys Rev A 85:062515
91. Shemer O, Brisker D, Moiseyev N (2005) Optimal reflection-free complex absorbing potentials for quantum propagation of wave packets. Phys Rev A 71(3):032716
92. McCurdy CW, Stroud C, Wisinski M (1991) Solving the time-dependent Schrödinger equation using complex-coordinate contours. Phys Rev A 43(11):5980–5990
93. Riss UV, Meyer HD (1995) Reflection-free complex absorbing potentials. J Phys B At Mol Opt 28(8):1475–1493
94. Sosnova KE, Telnov DA, Rozenbaum EB, Chu SI (2014) Exterior complex scaling method in TDDFT: HHG of Ar atoms in intense laser fields. J Phys Conf Ser 488(1):012022
95. Pohl A, Reinhard PG, Suraud E (2000) Towards single-particle spectroscopy of small metal clusters. Phys Rev Lett 84(22):5090–5093
96. Dinh PM, Romaniello P, Reinhard PG, Suraud E (2013) Calculation of photoelectron spectra: a mean-field-based scheme. Phys Rev A 87(3):032514
97. Caillat J, Zanghellini J, Kitzler M, Koch O, Kreuzer W, Scrinzi A (2005) Correlated multielectron systems in strong laser fields: a multiconfiguration time-dependent Hartree–Fock approach. Phys Rev A 71(1):012712
98. Scrinzi A (2012) t-SURFF: fully differential two-electron photo-emission spectra. New J Phys 14(8):085008
99. Tao L, Scrinzi A (2012) Photo-electron momentum spectra from minimal volumes: the time-dependent surface flux method. New J Phys 14(1):013021
100. Crawford-Uranga A, De Giovannini U, Mowbray DJ, Kurth S, Rubio A (2014) Modelling the effect of nuclear motion on the attosecond time-resolved photoelectron spectra of ethylene. J Phys B At Mol Phys 47(12):124018

101. De Giovannini U, Brunetto G, Castro A, Walkenhorst J, Rubio A (2013) Simulating pump-probe photoelectron and absorption spectroscopy on the attosecond timescale with time-dependent density functional theory. Chemphyschem 14(7):1363–1376
102. Gazibegović-Busuladžić A, Hasović E, Busuladžić M, Milosevic D, Kelkensberg F, Siu W, Vrakking M, Lepine F, Sansone G, Nisoli M, Znakovskaya I, Kling M (2011) Above-threshold ionization of diatomic molecules by few-cycle laser pulses. Phys Rev A 84(4): 043426